Supplement Information

# Engineering modular and tunable the overall photocatalytic generation of $H_2O_2$ via atomic regulation 1D Covalent Organic Frameworks

Machao Wang,[a] Kailun Yao,[a] Xiuyue He,[a] Shentong Jiang,[a] Zhiruo Tang,[a] Zhiyong Guo,*[,a] Jinni Shen*[,b] and Hongbing Zhan*[,a]

[a]College of Materials Science and Engineering, Fuzhou University, Fuzhou 350108, PR China

Email: guozhy@fzu.edu.cn; hbzhan@fzu.edu.cn

[b]State Key Lab of Photocatalysis on Energy and Environment, College of Chemistry, Fuzhou University, Fuzhou 350108, PR China

E-mail: t15067@fzu.edu.cn

## Materials and Methods

**Materials:** All solvents and reagents obtained from commercial sources were used without further purification. 1,4-dioxane (99%, AR), 1,3,5-trimethylbenzene (99%, AR), ethanol (EtOH, AR), tetrahydrofuran (THF, 99.5%), acetone (99%, AR), methanol (MeOH, AR), phenol (99%, AR) and 30% $H_2O_2$ stock solution were purchased from Sinopharm National Medicine Corporation. 2,3,6,7-tetrakis(4-formylphenyl)tetrathiafulvalene (TTF-4CHO, 99%), 4,4-diaminodiphenylsulfide (TAD, 99%), 4,4'-oxydiphenylamine (ODA, 99%), 4,4-diaminodiphenylmethane (MDA, 99%), potassium iodide (KI, 99%), potassium hydrogen phthalate ($C_8H_5KO_4$, 99%) and Rhodamine B (RhB, AR) were obtained from Adamas-Beta.

**Characterizations and instruments:** Fourier transform infrared spectra (FT-IR) in the region 4000-400 $cm^{-1}$ were tested using a Nicolet iS50 spectrometer with a KBr beam splitter. Powder X-ray diffraction (PXRD) patterns were collected on a Rigaku Miniflex 600, operated at 40 kV, 30 mA using Cu-Kα radiation (λ = 0.15416 nm) in Bragg-Brentano geometry. Thermogravimetric analyses (TGA) were performed on NETZSCH STA449-F5 by heating the samples from 35 to 900°C under a nitrogen atmosphere with a heating rate of 10 °C/min and a gas flow rate of 20 mL/min. The $^{13}$C-solidstate nuclear magnetic resonance ($^{13}$C-SS-NMR) spectra of the COF were measured by using a Bruker Advance III 500 nuclear magnetic resonance spectrometer. Scanning electron microscopy (SEM, Nova NanoSEM 230) was utilized to obtain the morphology of samples. The high-resolution transmission electron microscopy (HR-TEM) images of the samples were obtained by JEM-2100 Plus (LaB6 filament) at 200 kV. Nitrogen sorption isotherms analysis was performed at 77 K using Micromeritics ASAP 2020 Plus HD88 and all the samples (over 60 mg) were outgassed at 120°C for 12 h in a dynamic vacuum before measurements. The surface areas were calculated based on the Brunauer-Emmett-Teller (BET) model between $P/P_0$ values of 0.05 and 0.3.

**Synthesis of FZU-301:** 2,3,6,7-tetrakis(4-formylphenyl)tetrathiafulvalene (6.2 mg, 0.01 mmol) and 4,4-diaminodiphenylsulfide (3.9 mg, 0.02 mmol) were packed into a Pyrex tube (L = 20 cm, Φ = 10 mm), 0.4 mL 1,4-dioxane, 0.1 mL 6M AcOH, and 0.6 mL mesitylene were added into the Pyrex tube, the mixture was stirred and sonicated for 15 min. Then the Pyrex tube was degassed through freeze-pump-thaw cycles for three times, and flame sealed to an approximate length of 15 cm. The reaction was heated to 120℃ for 5 d. After the reaction, the Pyrex tube was opened using a glass cutter, the solid was collected by filtration and washed with acetone, and then the solid was washed with tetrahydrofuran in a Soxhlet extractor for 1 day and dried under vacuum at 120℃ to obtain 8.6 mg of purple-red solid (yield: 86%).

**Synthesis of FZU-302:** 2,3,6,7-tetrakis(4-formylphenyl)tetrathiafulvalene (6.2 mg, 0.01 mmol) and 4,4'-oxydiphenylamine (4 mg, 0.02 mmol) were packed into a Pyrex tube (L = 15 cm, Φ = 10 mm), 0.4 mL 1,4-dioxane, 0.1 mL 6M AcOH, and 0.6 mL mesitylene were added into the Pyrex tube, the mixture was stirred and sonicated for 15 min. Then the Pyrex tube was degassed through freeze-pump-thaw cycles for three times, and flame sealed to an approximate length of 15 cm. The reaction was heated to 120℃ for 5 d. After the reaction, the Pyrex tube was opened using a glass cutter, the solid was collected by filtration and washed with acetone, and then the solid was washed with tetrahydrofuran in a Soxhlet extractor for 1 day and dried under vacuum at 120℃ to obtain 8.9 mg of purple-black solid (yield: 88%).

**Synthesis of FZU-303:** 2,3,6,7-tetrakis(4-formylphenyl)tetrathiafulvalene (6.2 mg, 0.01 mmol) and 4,4-diaminodiphenylmethane (3.9 mg, 0.02 mmol) were packed into a Pyrex tube (L = 20 cm, Φ = 10 mm), 0.4 mL 1,4-dioxane, 0.1 mL 6M AcOH, and 0.6 mL mesitylene were added into the Pyrex tube, the mixture was stirred and sonicated for 15 min. Then the Pyrex tube was degassed through freeze-pump-thaw cycles for three times, and flame sealed to an approximate length of 15 cm. The reaction was heated to 120℃ for 5 d. After the reaction, the Pyrex tube was opened using a glass cutter, the solid was collected by filtration and washed with acetone, and

then the solid was washed with tetrahydrofuran in a Soxhlet extractor for 1 day and dried under vacuum at 120℃ to obtain 8.5 mg of purple-red solid (yield: 84%).

**Photoelectrochemical measurements:** All electrochemical measurements (photocurrent, Mott Schottky and EIS) were made in 0.2 M sodium sulfate solution (pH = 6.8) through the traditional three electrode system in the INTERFACE 1000E electrochemical workstation[1].The working electrode is ITO glass plate coated with catalyst slurry, the counter electrode is platinum foil, and saturated Ag/AgCl as reference electrode. Mott Schottky plots were measured at alternating current (AC) frequencies of 1000 Hz ,1500 Hz and 2000 Hz[2].

**Preparation of working electrode:** 2 mg catalyst, 1 mL ethanol and 10 μL Nafion D-520 were mixed and ultrasound for 30 min. Then, 200 μL slurry solution was deposited evenly on the ITO glass plate (1 × 2 $cm^2$) and left to dry in the air.

**Photocatalytic reactions:** In a typical experiment, the photosynthesis of $H_2O_2$ was carried out in 25 mL glass tube containing 5 mg COF and 10 mL deionized water at 25℃ under $O_2$ atmosphere. Then, the solution was irradiated with a xenon lamp source (PLS-SXE300D, Beijing Perfect Light). The $H_2O_2$ content in the solution was evaluated every 15 min.

**$H_2O_2$ detection methods (iodometry):** The amount of $H_2O_2$ was analyzed by iodometry. 1 mL 0.1 mol $L^{-1}$ potassium hydrogen phthalate ($C_8H_5KO_4$) aqueous solution and 1 mL 0.4 mol $L^{-1}$ potassium iodide (KI) potassium hydrogen phthalate ($C_8H_5KO_4$) aqueous solution and 1 mL 0.4 mol $L^{-1}$ potassium iodide (KI) iodine ions ($I^-$) under acidic conditions to generate triiodide ions ($I_3^-$), which have strong absorption near 350 nm. The absorbance of $I_3^-$ at 350 nm is measured by ultraviolet spectrophotometer (UH5300). Therefore, the amount of $H_2O_2$ generated by each reaction can be calculated.

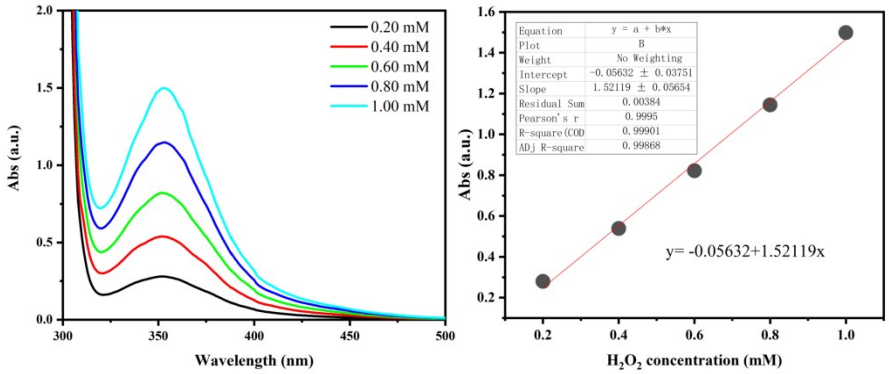


**In-situ Fourier transform infrared spectrometer (FT-IR) analysis**: In-situ Fourier transform infrared spectrometry was performed on a Nicolet iS-50 instrument. The sample was filled into an in-situ IR cell, and $O_2$ and $H_2O$ vapors were introduced into the cell and fiber source (FX300, Beijing Perfect Light Technology Co., Ltd., Beijing, China) through the $CaF_2$ window of the cell. Before the measurement, the samples were degassed at 423 K for 4 h. The baseline was obtained before the sample reached $O_2$ adsorption equilibrium within 1 h[3].

**EPR measurements:** Electron paramagnetic spectroscopy (EPR) was measured on a Bruker EMX plus model spectrometer. The generation of reactive species including photogenerated electrons ($e^-$), superoxide radicals ($^{\bullet}O_2^-$), and hydroxyl radicals ($^{\bullet}OH$) by COFs during the $H_2O_2$ photosynthesis process were investigated by EPR measurements. 5,5-dimethyl-1-pyrroline N-oxide (DMPO) and 4-hydroxy-2,2,6,6-tetramethylpiperidinyloxy (TEMPO) were used as the spin trapping agents. 1 μL DMPO was added into 50 μL sample suspension (1 g/L in DMSO) for the detection of $^{\bullet}O2^-$. 1 μL DMPO was added into 100 μL sample suspension (1 g/L in water) for the detection of $^{\bullet}OH$. Additionally, 1 μL TEMPOL (2.5 mM) was added into 200 μL sample suspension (1 g/L in water) for the detection of $e^-$. The mixed suspensions were placed into the quartz capillary tube and then irradiated by visible-light to detect the signal intensity of the spin capture adduct.

**Room-temperature photoluminescence (PL) measurement:** PL measurement was measured on FLS1000 fluorescence spectrophotometer. The solid sample is placed on the substrate. A monochromatic light source (e.g., a 450 nm laser diode) is used for steady-state excitation. The emitted PL signal from the sample is collected and directed into a spectrometer. It is then dispersed and detected by a charge-coupled device (CCD) detector. Finally, the spectrum is acquired and plotted as intensity versus wavelength (nm). This provides information on the optical bandgap and impurity states.

**Variable-temperature photoluminescence (PL) spectroscopy:** The test equipment is FLS1000 fluorescence spectrophotometer. Variable-temperature photoluminescence (PL) spectroscopy is performed by mounting the sample in a closed-cycle cryostat or a temperature-controlled stage. The sample temperature is precisely varied, typically from 80 K to 300 K or higher. At each stabilized temperature, the sample is excited by a laser, and the emitted PL signal is collected and analyzed by a spectrometer equipped with a CCD or InGaAs detector. This technique maps the evolution of emission peak energy, intensity, and linewidth with temperature, providing critical insights into exciton dynamics, defect states, and carrier recombination mechanisms.

**Time-resolved photoluminescence (TRPL) measures the fluorescence:** The test equipment is FLS1000 fluorescence spectrophotometer. TRPL measures the fluorescence decay lifetime. A pulsed laser (e.g., picosecond or nanosecond pulses) excites the sample. The subsequent emission decay is detected by a fast-response photodetector, such as a photomultiplier tube. The time-dependent intensity is recorded using time-correlated single-photon counting (TCSPC) or a streak camera system. The decay curve is then fitted to exponential models, extracting lifetime constants ($\tau$) on the nanosecond to microsecond scale. This reveals dynamics of radiative recombination, energy transfer, and quenching processes.

**The AQY and SCC measurement:** The photocatalytic reaction was carried out in pure deionized water (100 mL) and catalyst (50 mg) in a photocatalytic reactor. After sonication and bubbling, the bottle was irradiated by a Xe lamp at 420-800 nm (Beijing Perfect Light Technology Co., LTD., Beijing, China).

The apparent quantum yield (AQY) of the photocatalyst was measured under the irradiation of a 300 W Xe lamp with a 420 nm band-pass filter. The active area of the reactor is about 11.34 $cm^2$. Use PL-MW2000 optical radiometer to take the average value of monochromatic light intensity at three representative points. Therefore, the light intensity at 420 nm is calculated as 20.3 mW $cm^{-2}$. AQY is calculated as follows:

$$AQY = \frac{(Number\ of\ produced\ H_2O_2\ mulecules) \times 2}{Number\ of\ incident\ photons} \times 100\%$$

$$AQY = \frac{(M_{H_2O_2} \times N_A \times h \times c)}{S \times P \times T \times \lambda} \times 100$$

**M =** yield of $H_2O_2$ (mol);

**NA (Avogadro constant) =** $6.02 \times 10^{23}$ $mol^{-1}$;

**h (Planck constant) =** $6.626 \times 10^{-34}$ J·s;

**c (Speed of light) =** $3 \times 10^8$ m/s;

**S = Irradiation area ($cm^2$) =** 11.5 $cm^2$;

**P = the intensity of irradiation light (W / $cm^2$) =** 59.6 mW / $cm^2$ (420 nm);

**T = the photoreaction time (s) =** 3600 s;

**λ = the wavelength of the monochromatic light (nm) =** $420 \times 10^{-9}$ m;

**The SCC efficiency was calculated by the following equation:**

$$SCC\ efficiency\ (\%) = \frac{[\Delta G\ for\ H_2O_2\ generation\ (J\ mol^{-1}) \times [H_2O_2\ formed\ (mol)]}{[Total\ input\ power\ (W) \times [Reation\ time\ (s)]} \times 100$$

where ΔG = 117 kJ $mol^{-1}$, the irradiated area is 11.5 $cm^2$, the total input energy was therefore 1.15 W.

**Photocatalytic evolution of $^{\bullet}O_2^-$:** NBT (nitro blue tetrazolium) method. 15 mg catalysts were suspended in 50 mL NBT aqueous solution with a concentration of 2.0 $\times 10^{-5}$ M. The light source was consistent with the above light source used in the photocatalytic reaction, and the overall experimental photocatalyst was separated with

a 0.22 μm filter. The absorbance of the supernatant was measured on a spectrophotometer. The generation of $^{\bullet}O_2^-$ was determined by the degradation of NBT, which was detected by the absorbance change at the wavelength of 259 nm[3].

**Detect $^1O_2$ by DPBF**：1 mg COFs (1D TTF COFs, respectively), 4 mL water, and 4 mL DPBF solution (0.05 mM, DMF as solvent) were mixed and dispersed in a quartz tube. The quartz tube was illuminated by 300 W xenon lamp and cooled by circulating water. After irradiation, the supernatant was collected by centrifugation, and the UV-Vis spectra were collected[4].

**Transient absorption (TA) measurements:** Femtosecond (fs) transient absorption spectroscopy measurements were investigated by a Pharos ultrafast Yb: KGW laser (Light Conversion) with a regenerative amplifier, which produces IR pulses (10 W) centered at 1030 nm wavelength (200 kHz, pulse width < 290 fs). A portion of this beam (80%) was sent through an optical parametric amplifier (OPA, ORPHEUS, Light Conversion) to generate 370 nm pump beam for the excitation (pulse duration ~70 fs), and the residual was used as the probe beam. The resulting pump and probe pulses were directed into a TA spectrometer (Harpia, Light Conversion). Both the pump and probe pulses were sent into an optical bench. The probe pulse was focused into a sapphire crystal, generating a continuum white light as the probe light. The frequency of the pump pulse was reduced to 95 Hz, using a chopper, and the absorption with and without pumping light was measured and compared. For TA measurements in the time domain of 100 ps, a time delay of the probe pulse with respect to the pump pulse was regulated by a computer-controlled optical delay stage. Pump and probe pulses were focused and overlapped on the sample plane, which was housed in a 1 mm cuvette. The transmitting white-light probe pulses were directed into a photodiode array detector (Kymera, Andor). The resulting absorption differences were calibrated and analyzed using software (Harpia service app, Light Conversion). Samples with an optical absorbance of 3.0 in $H_2O$ (3 mL) and ethylene glycol (0.2 mL) were used[5].

**DFT calculations:** All density functional theory (DFT) calculations were performed using the Vienna Ab initio Simulation Package (VASP).[6,7] The exchange-correlation interactions were treated within the generalized gradient approximation (GGA) using the revised Perdew–Burke–Ernzerhof (PBE) functional.[8] The projector-augmented wave (PAW) method[9] was employed to describe electron-ion interactions, and a plane-wave basis set with an energy cutoff of 500 eV was used. Van der Waals interactions were accounted for using Grimme's DFT-D3 empirical dispersion correction.[10] The Brillouin zone was sampled with a Γ-centered 1 × 5 × 1 k-point mesh. All atomic positions were fully relaxed until the Hellmann-Feynman forces on each atom were less than 0.05 $eV \cdot Å^{-1}$ and the energy difference between successive electronic steps were below $10^{-6}$ eV. A vacuum layer of at least 20 Å was added along the non-periodic direction to eliminate interactions between periodic images. Bader charge analysis was performed based on the calculated electron density to evaluate atomic charges.[11]

The Gibbs free energy change (ΔG) for each chemical reaction was calculated using the equation $\Delta G = \Delta E_{DFT} + \Delta ZPE - T\Delta S$, where $\Delta E_{DFT}$, ΔZPE, T, and ΔS represent the change in DFT-calculated total energy, the change in zero-point energy, the temperature (298.15 K), and the change in entropy, respectively.

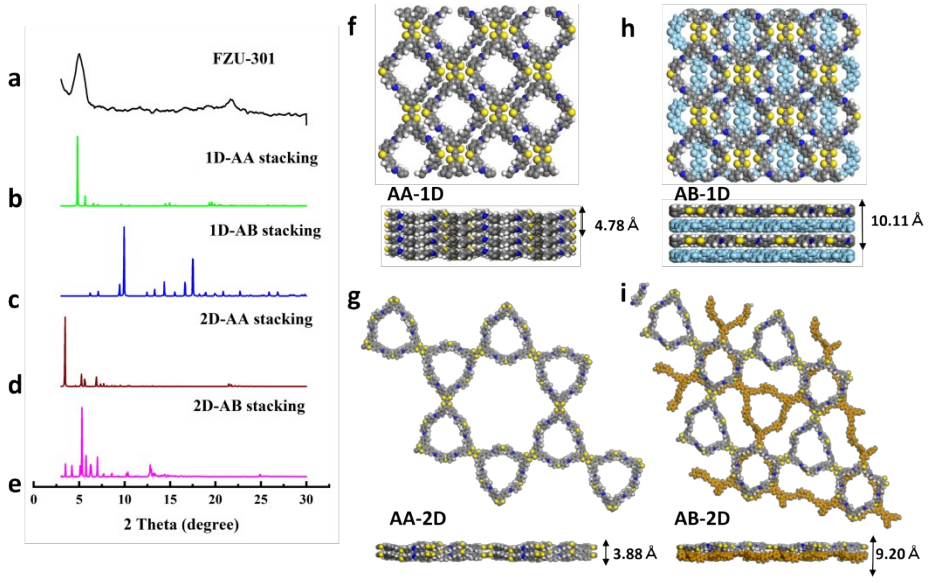


**Figure S1.** (a) Experimentally PXRD pattern, simulated PXRD patterns for (b) AA-1D structure, (c) AB-1D structure, (d) AA-2D structure, (e) AB-2D structure. Those structures with their unit cell parameters of AA-1D (f), AB-1D (g), AA-2D (h), and AB-2D (i). All the data were contributed by FZU-301. The simulated PXRD pattern of AA-1D structure shows a high similarity with the experimental results.

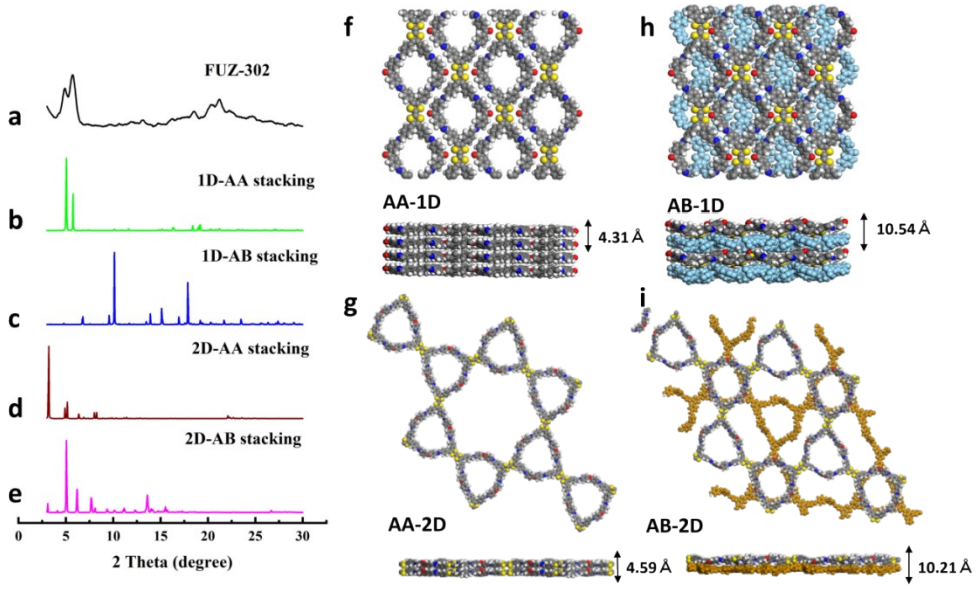


**Figure S2.** (a) Experimentally PXRD pattern, simulated PXRD patterns for (b) AA-1D structure, (c) AB-1D structure, (d) AA-2D structure, (e) AB-2D structure. Those structures with their unit cell parameters of AA-1D (f), AB-1D (g), AA-2D (h), and AB-2D (i). All the data were contributed by FZU-302. The simulated PXRD pattern

of AA-1D structure shows a high similarity with the experimental results.

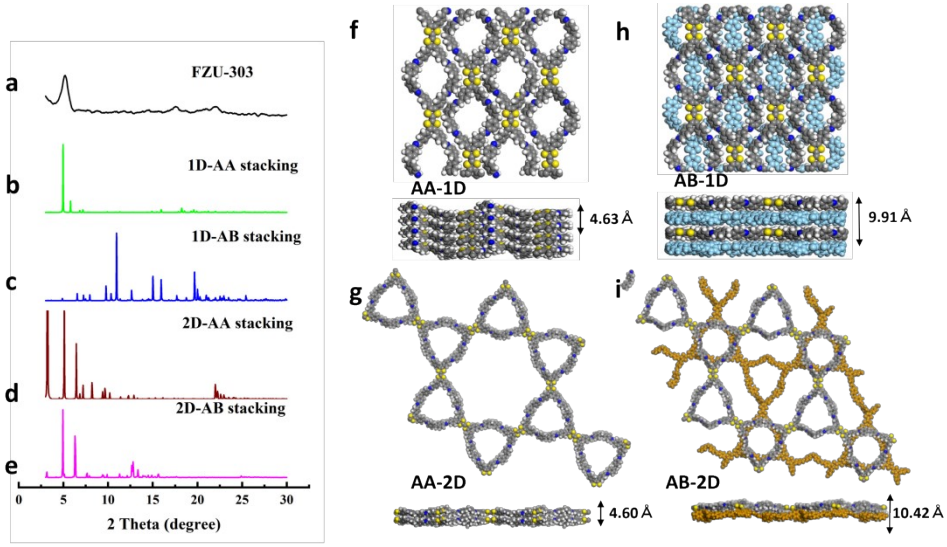


**Figure S3.** (a) Experimentally PXRD pattern, simulated PXRD patterns for (b) AA-1D structure, (c) AB-1D structure, (d) AA-2D structure, (e) AB-2D structure. Those structures with their unit cell parameters of AA-1D (f), AB-1D (g), AA-2D (h), and AB-2D (i). All the data were contributed by 1D TTF COF-3. The simulated PXRD pattern of AA-1D structure shows a high similarity with the experimental results.

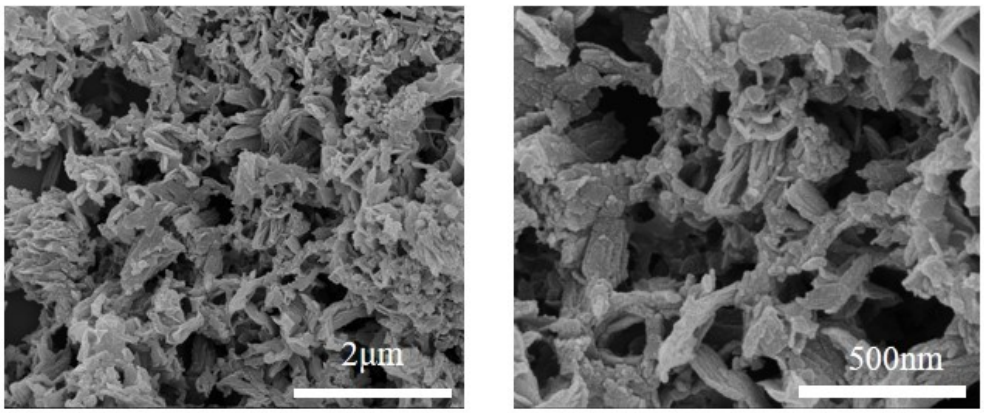


**Figure S4.** SEM images of FZU-302.

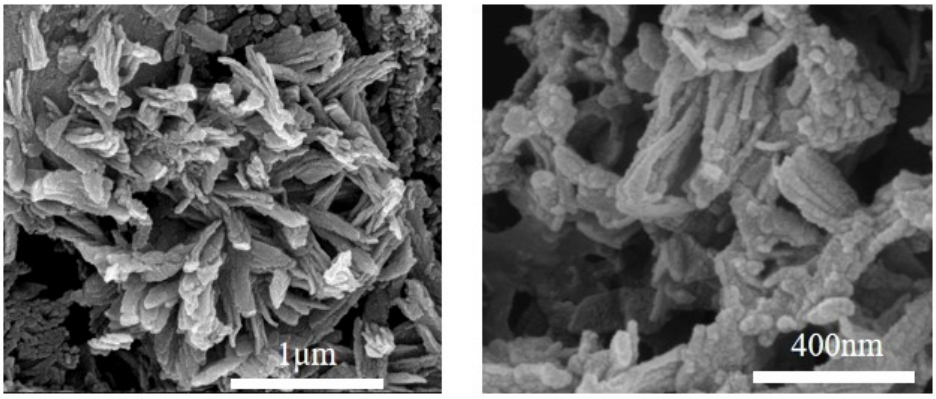


.

**Figure S5.** SEM images of FZU-303.

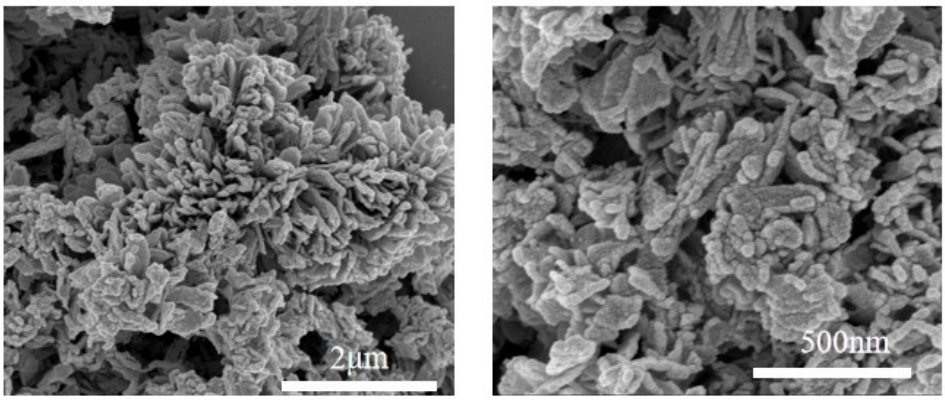


**Figure S6.** SEM images of FZU-301.

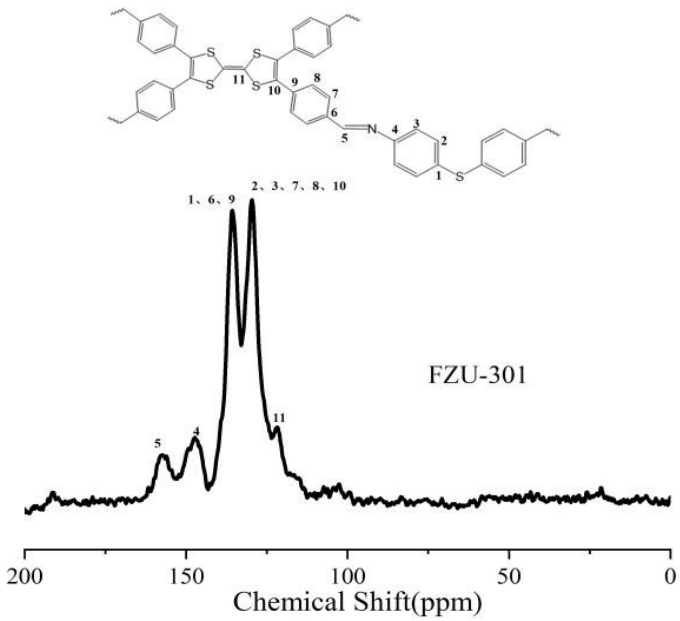


**Figure S7.** $^{13}C$ ssNMR spectrum of FZU-301.

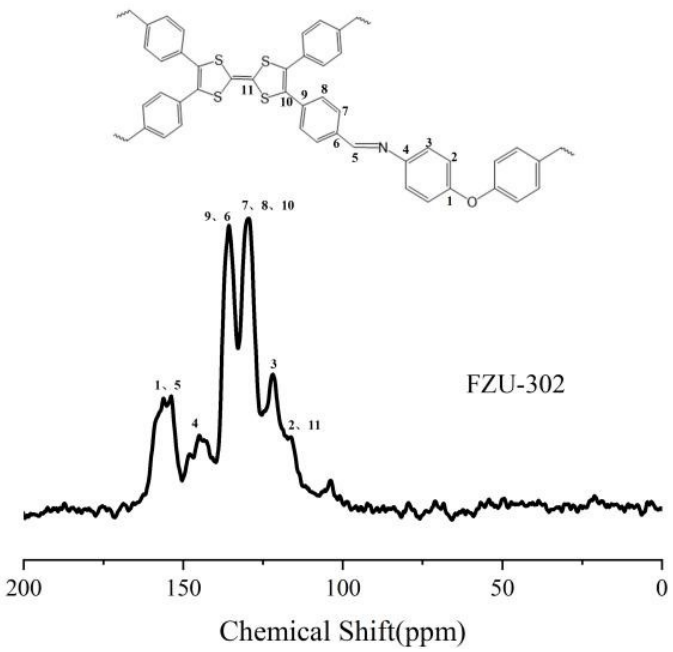


**Figure S8.** $^{13}C$ ssNMR spectrum of FZU-302.

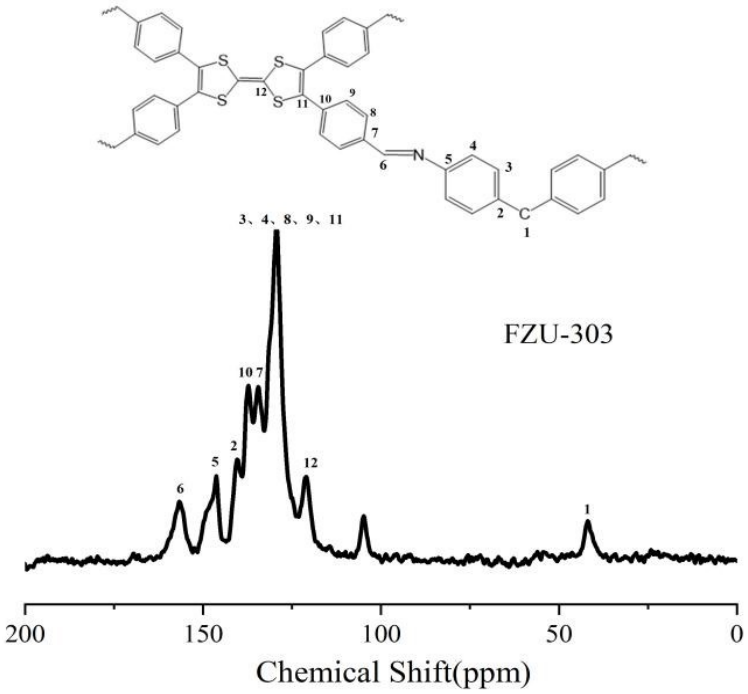


**Figure S9.** $^{13}C$ ssNMR spectrum of FZU-303.

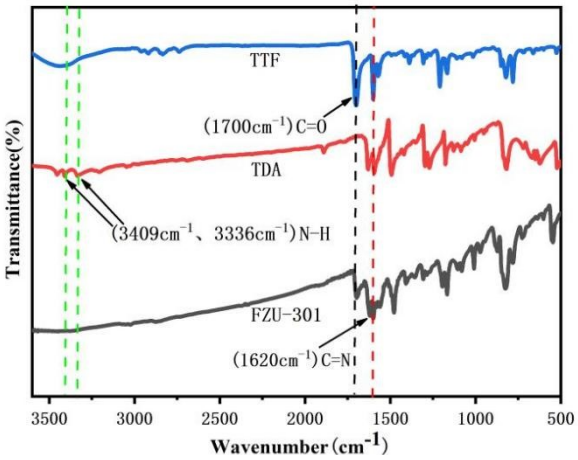


**Figure S10.** The FT-IR spectra of FZU-301.

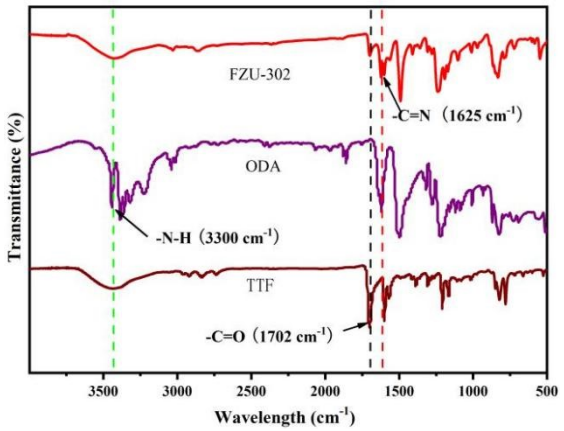


**Figure S11.** The FT-IR spectra of FZU-302.

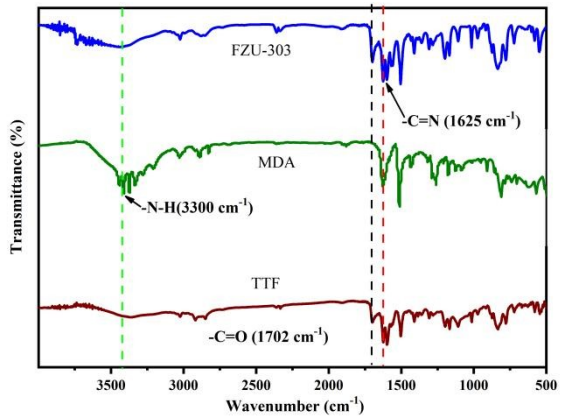


**Figure S12.** The FT-IR spectra of FZU-303.

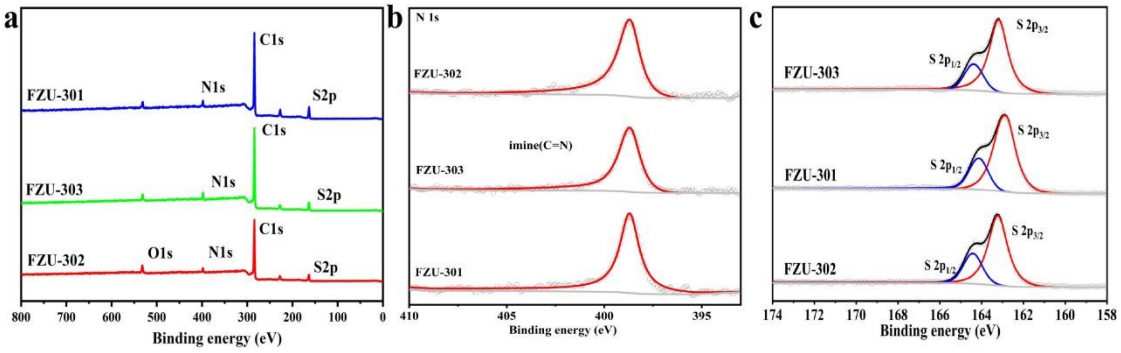


**Figure S13.** (a) Total XPS spectra; (b) N 1s; (c) S 2p.

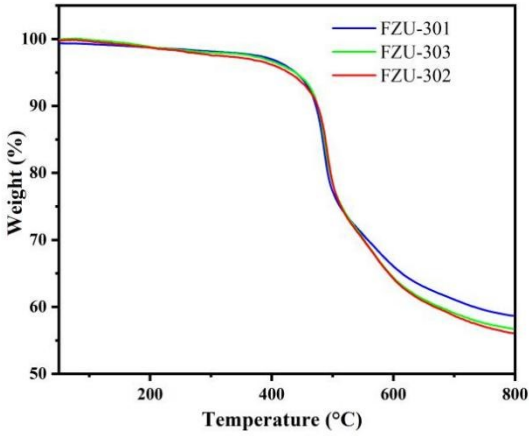


**Figure S14.** TGA curves of COFs under $N_2$ atmosphere. All of the three COFs showed excellent thermal stability.

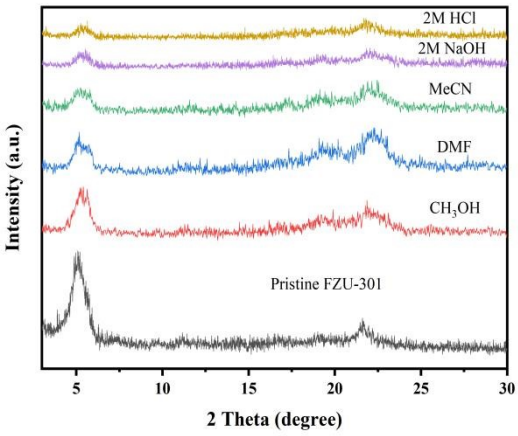


**Figure S15.** The PXRD curves of FZU-301 after treatment in different media for 5 days.

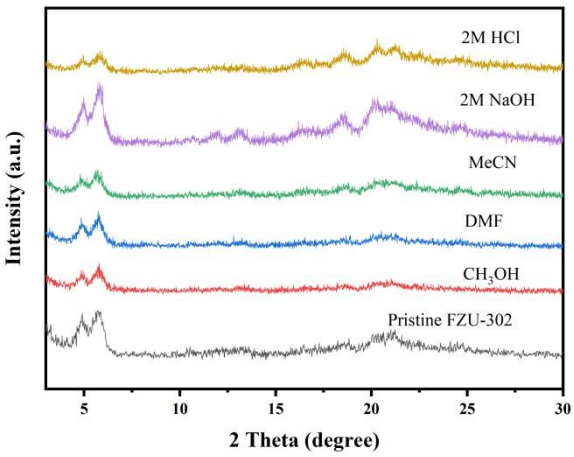


**Figure S16.** The PXRD curves of FZU-302 after treatment in different media for 5 days.

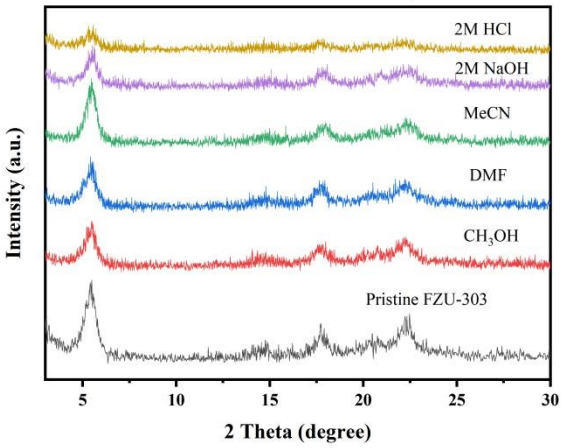


**Figure S17.** The PXRD curves of FZU-303 after treatment in different media for 5 days.

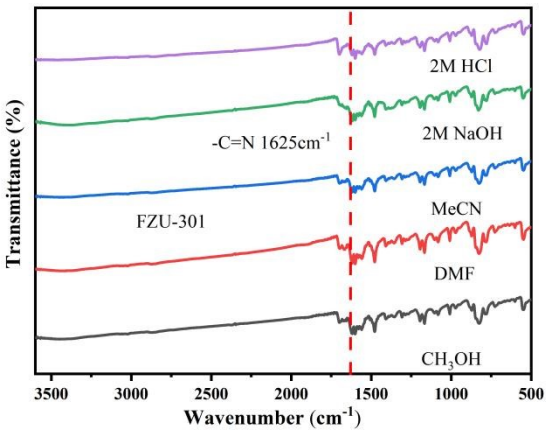


**Figure S18.** FT-IR patterns of FZU-301 after treatment in different media for 5 days.

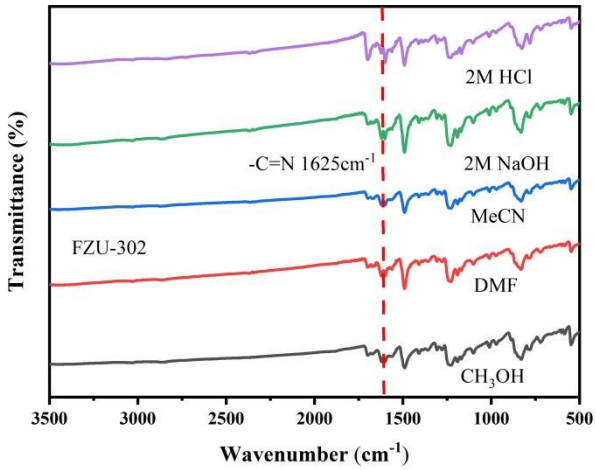


**Figure S19.** FT-IR patterns of FZU-302 after treatment in different media for 5 days.

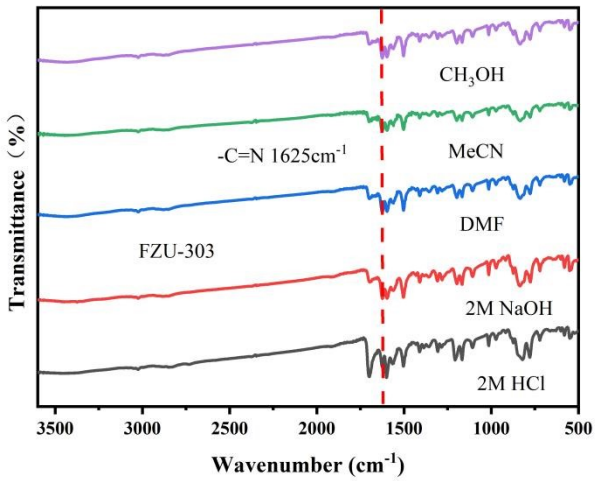


**Figure S20.** FT-IR patterns of FZU-303 after treatment in different media for 5 days.

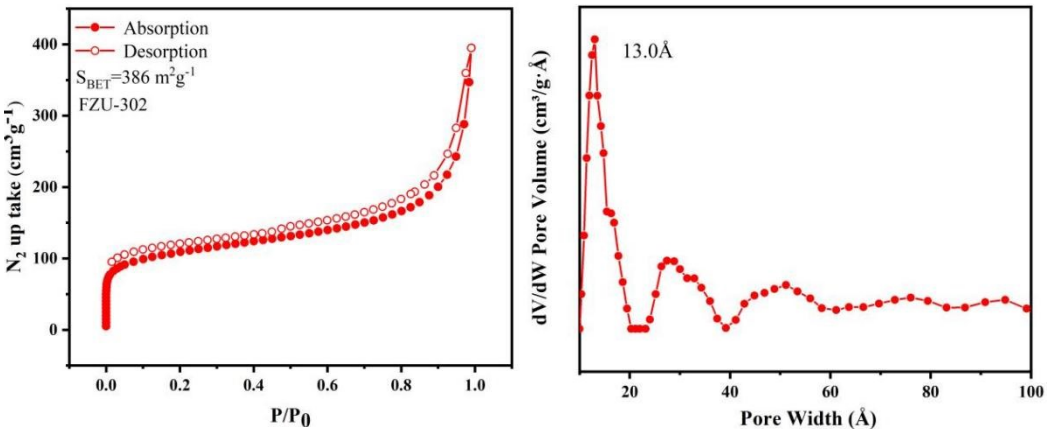


**Figure S21.** $N_2$ adsorption-desorption isotherms and pore size distribution for FZU-302.

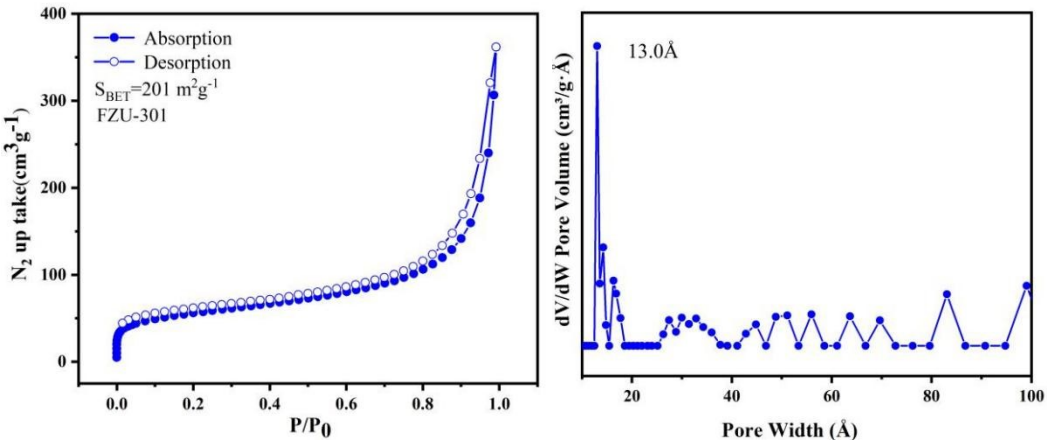


**Figure S22.** $N_2$ adsorption-desorption isotherms and pore size distribution for FZU-301.

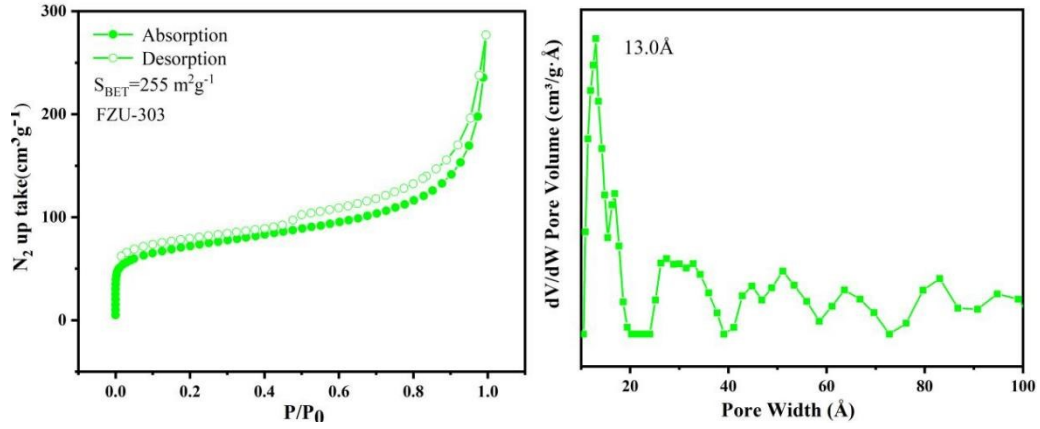


**Figure S23.** $N_2$ adsorption-desorption isotherms and pore size distribution for FZU-303.

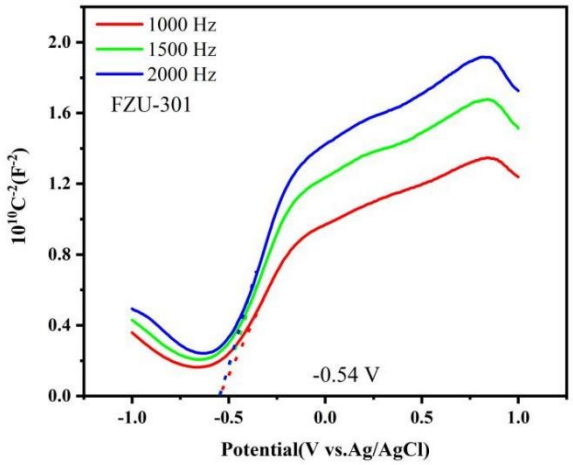


**Figure S24.** Mott-Schottky plots of FZU-301.

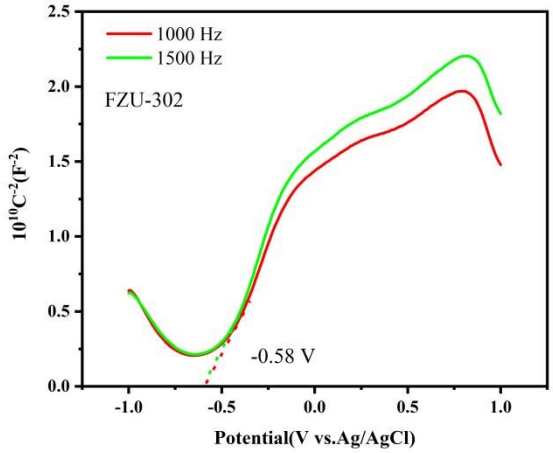


**Figure S25.** Mott-Schottky plots of FZU-302.

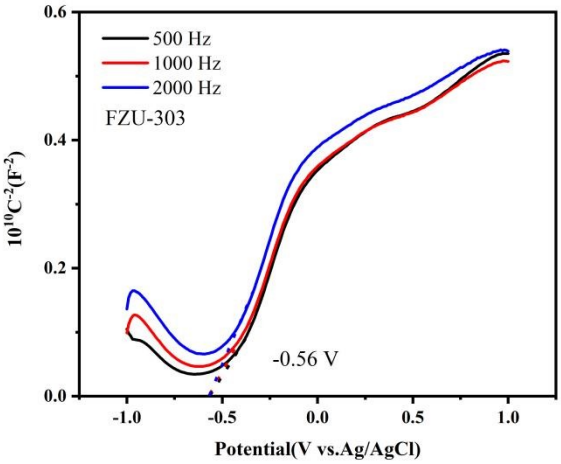


**Figure S26.** Mott-Schottky plots of FZU-303.

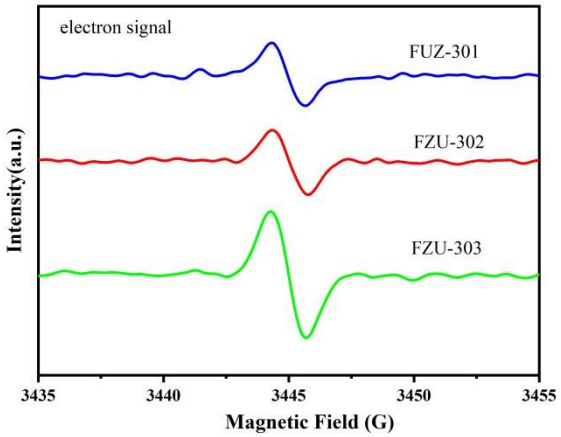


**Figure S27.** EPR spectra of 1D COFs under visible light.

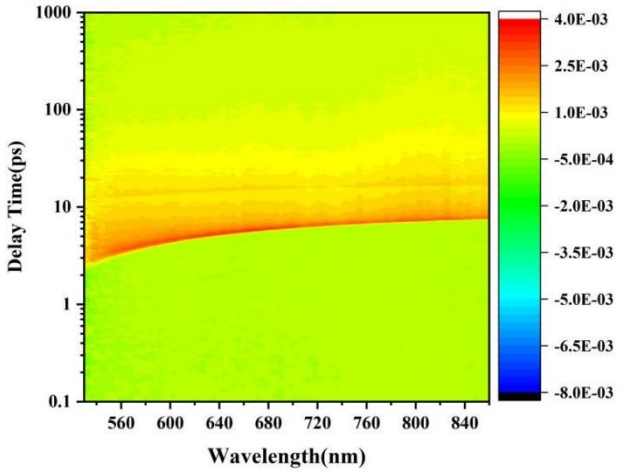


**Figure S28.** fs-TAS data maps of FZU-302 with 400 nm excitation.

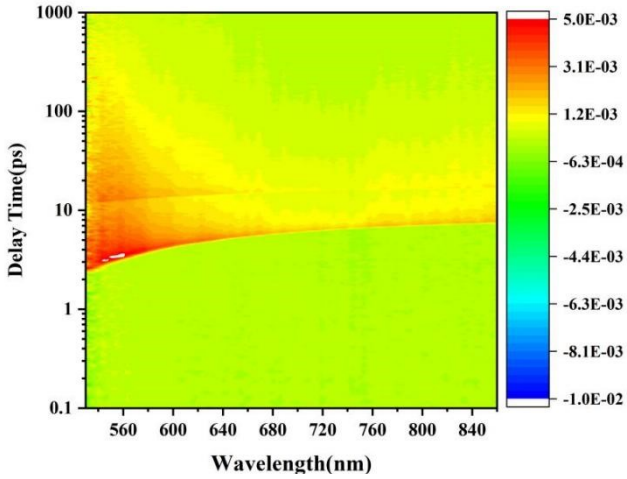


**Figure S29.** fs-TAS data maps of FZU-303 with 400 nm excitation.

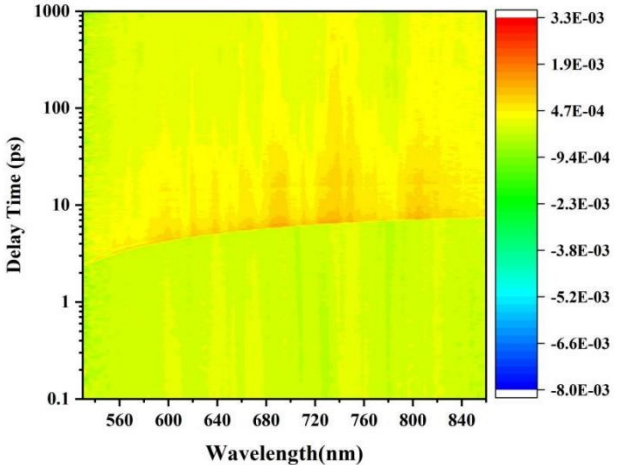


**Figure S30.** fs-TAS data maps of FZU-301 with 400 nm excitation.

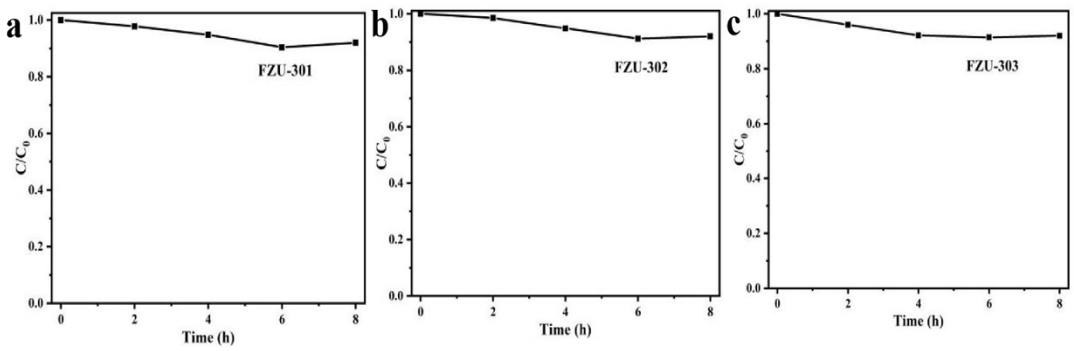


**Figure S31.** Photostability of $H_2O_2$ aqueous solution containing 1D COFs under $N_2$ atmosphere. The initial $H_2O_2$ concentration was 1 mM.

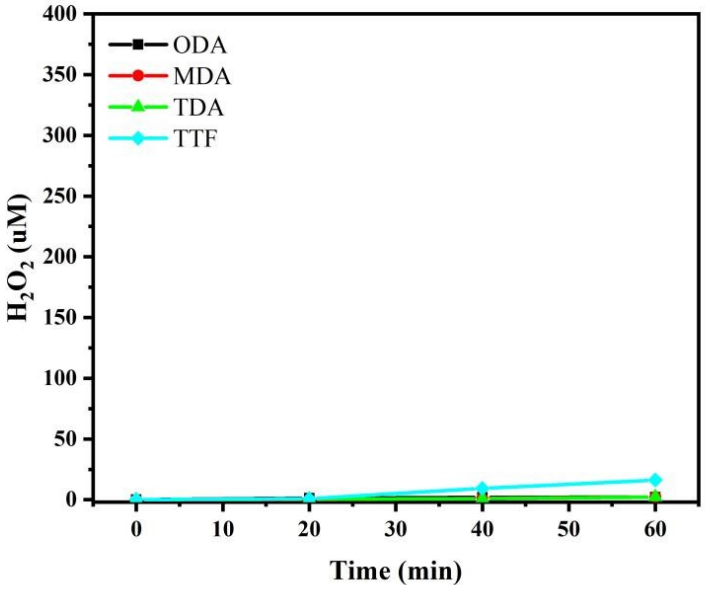


**Figure S32.** Photocatalytic $H_2O_2$ yield by the monomers of COFs (Reaction condition: 5 mg catalyst in 10 mL pure water, $\lambda > 420$ nm 300 W Xe lamp.

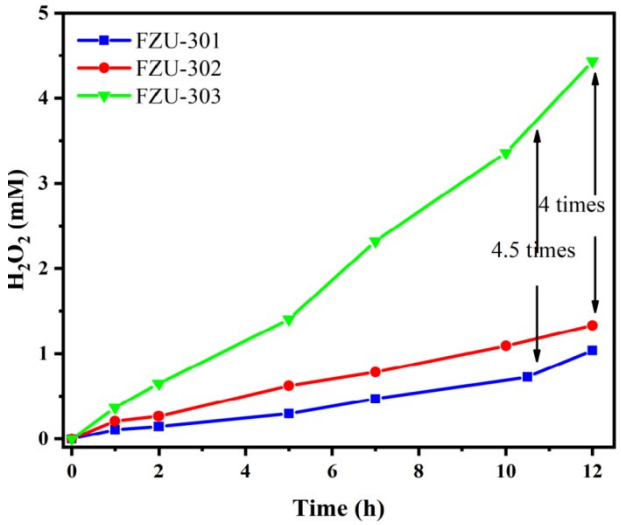


**Figure S33.** Long time $H_2O_2$ accumulation generated by 1D COFs photocatalysts.

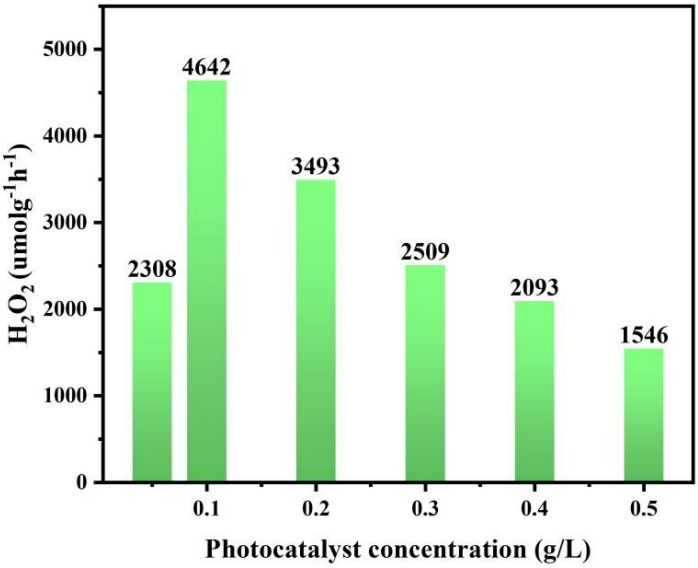


**Figure S34.** Photocatalytic $H_2O_2$ yield of FZU-303 with different catalyst concentrations.

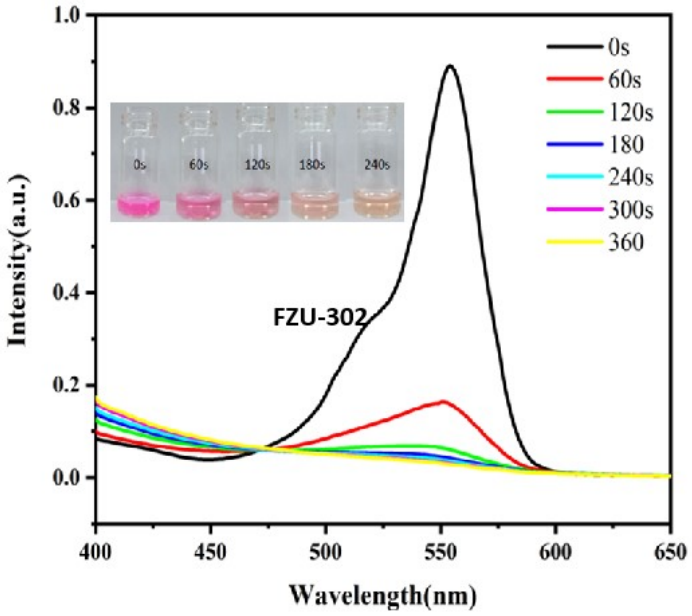


**Figure S35.** In-situ UV-vis spectra of waste water containing RhB (10 mg/L) degraded with the as-synthesized $H_2O_2$ solution that photocatalyzed by FZU-302.

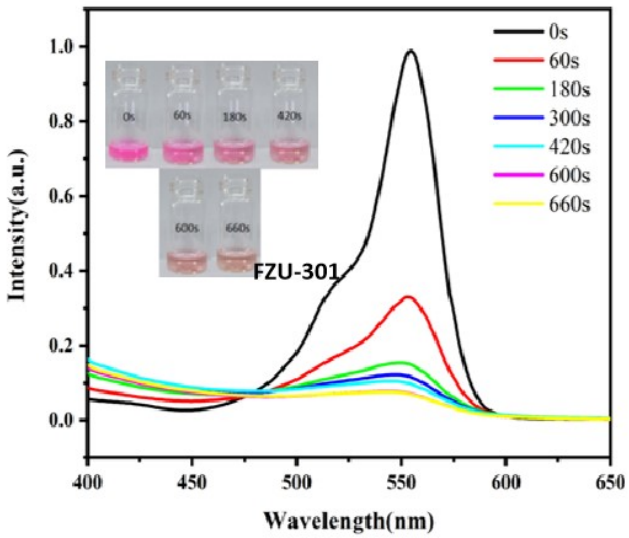


**Figure S36.** In-situ UV-vis spectra of waste water containing RhB (10 mg/L) degraded with the as-synthesized $H_2O_2$ solution that photocatalyzed by FZU-301.

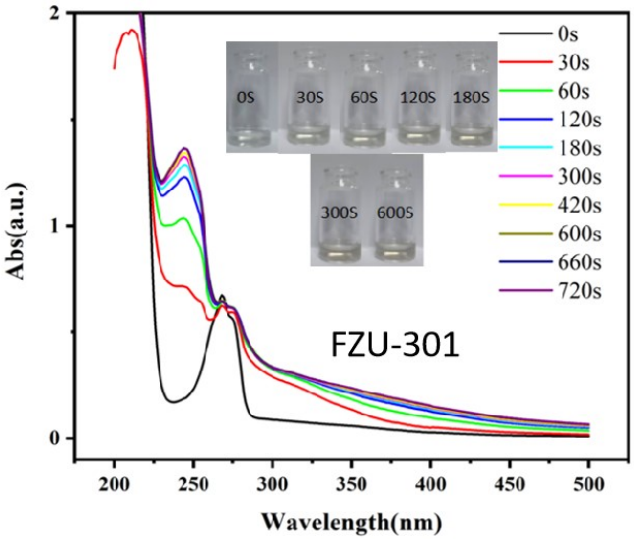


**Figure S37.** In-situ UV-vis spectra of waste water containing phenol (10 mg/L) degraded with the as-synthesized $H_2O_2$ solution that photocatalyzed by FZU-301.

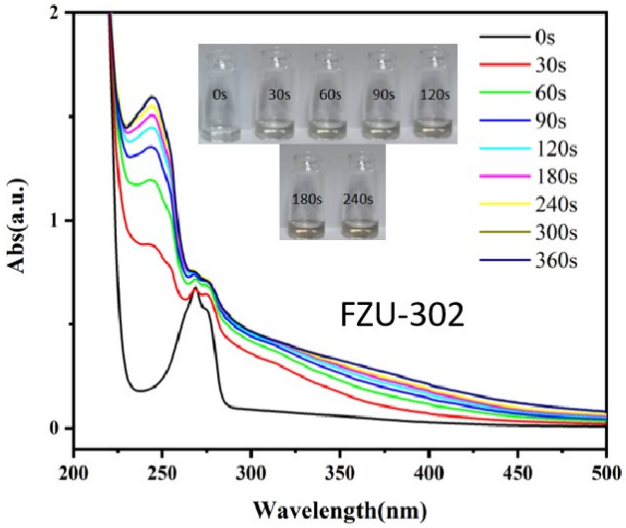


**Figure S38.** In-situ UV-vis spectra of waste water containing phenol (10 mg/L) degraded with the as-synthesized H2O2 solution that photocatalyzed by FZU-302.

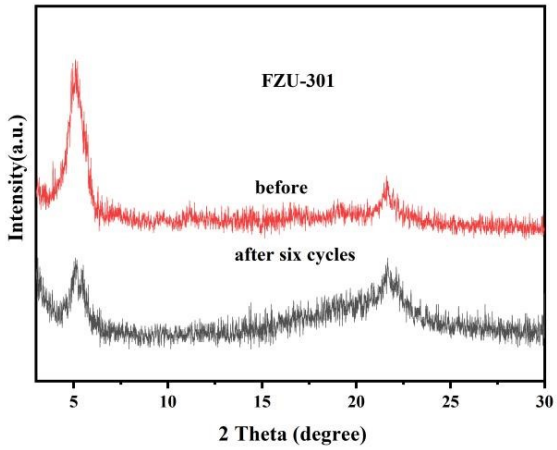


**Figure S39.** PXRD patterns of FZU-301 before and after photocatalytic reactions.

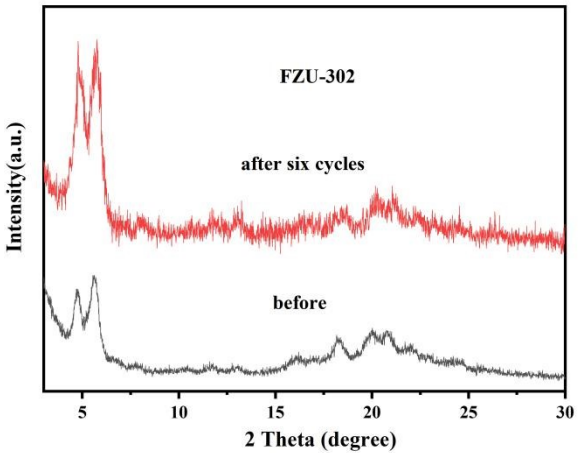


**Figure S40.** PXRD patterns of FZU-302 before and after photocatalytic reactions.

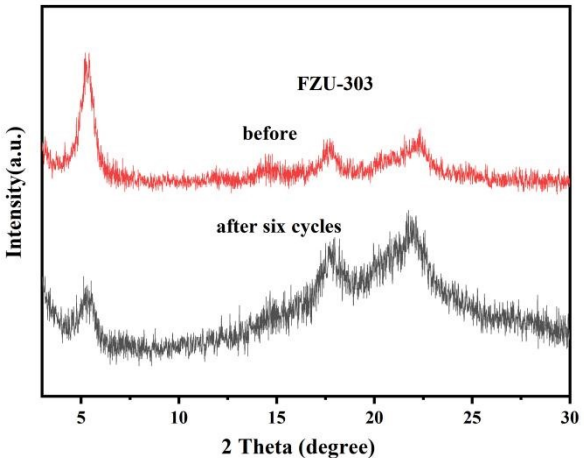


**Figure S41.** PXRD patterns of FZU-303 before and after photocatalytic reactions.

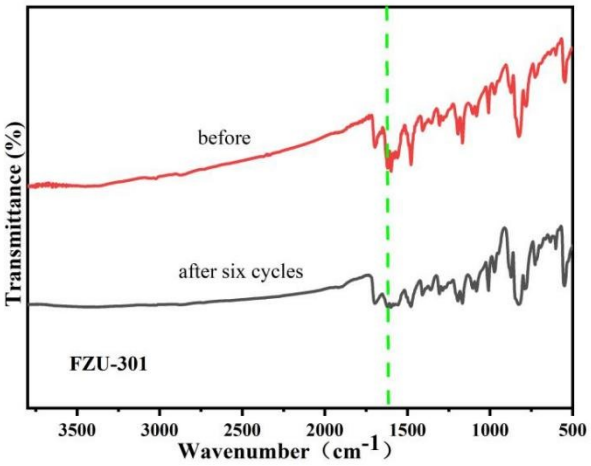


**Figure S42.** FT-IR patterns of FZU-301 before and after photocatalytic reactions.

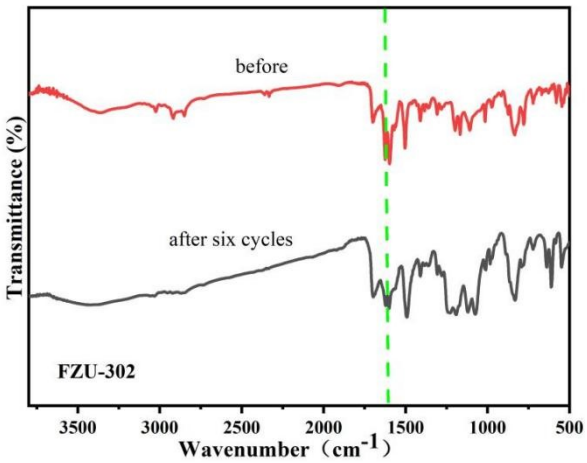


**Figure S43.** FT-IR patterns of FZU-302 before and after photocatalytic reactions.

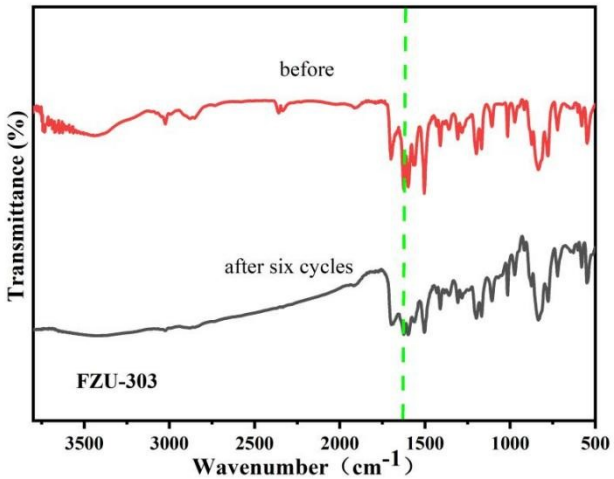


**Figure S44.** FT-IR patterns of FZU-303 before and after photocatalytic reactions.

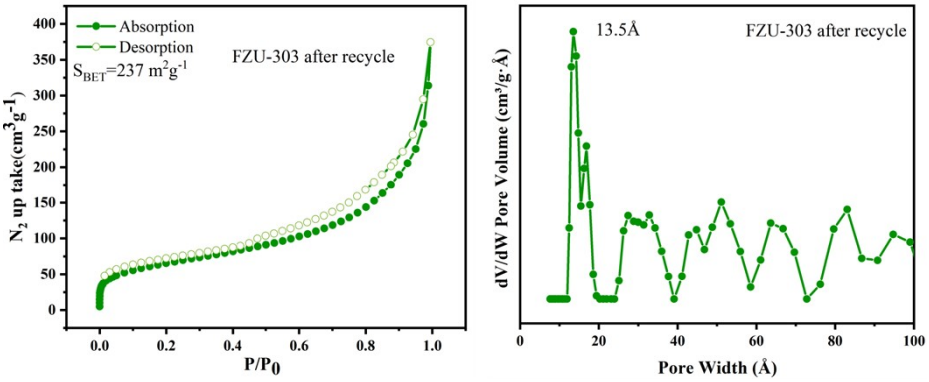


**Figure S45.** BET of FZU-303 after photocatalytic reactions.

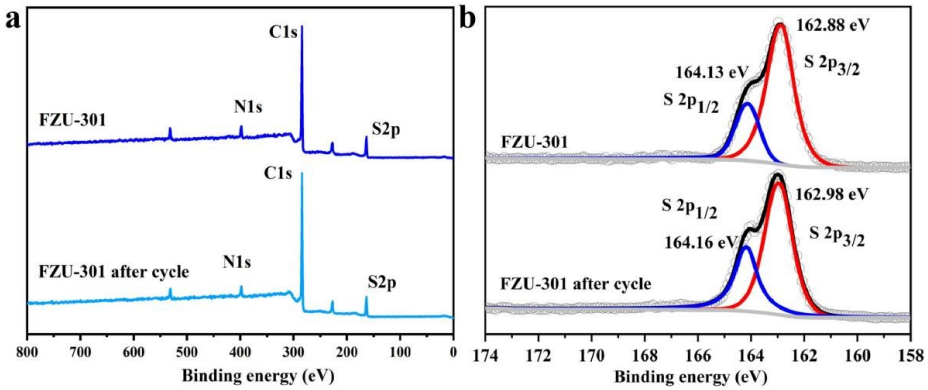


**Figure S46.** The XPS spectra of FZU-301 before and after the cycle (a) the total form and (b) the S 2p fine spectrum.

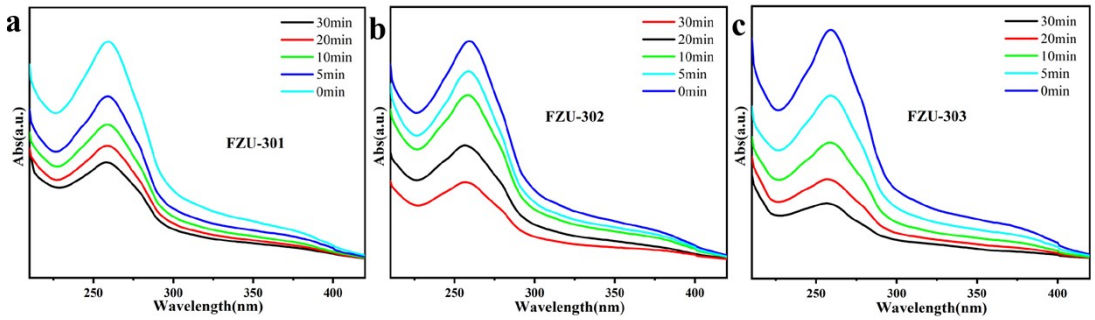


**Figure S47.** The photocatalytic experiment of $^{\bullet}O_2^-$ on COFs detected by NBT method.

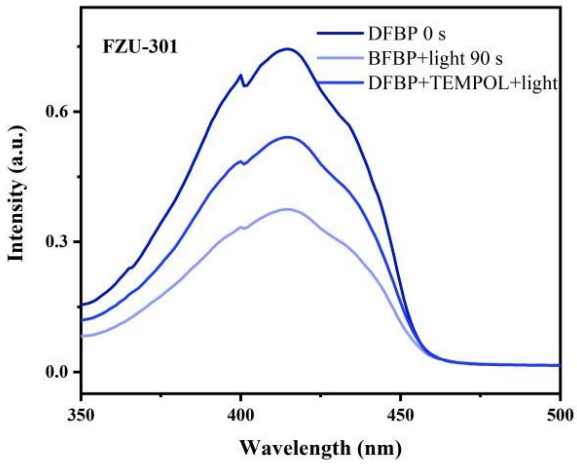


**Figure S48.** The photocatalytic experiment of $^1O_2$ on FZU-301 detected by DPBF method.

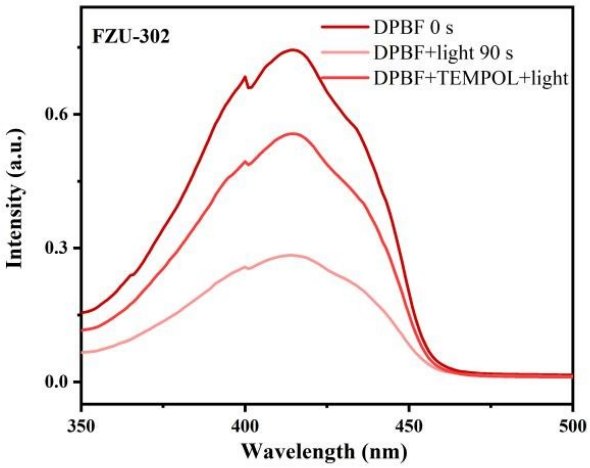


**Figure S49.** The photocatalytic experiment of $^1O_2$ on FZU-302 detected by DPBF method.

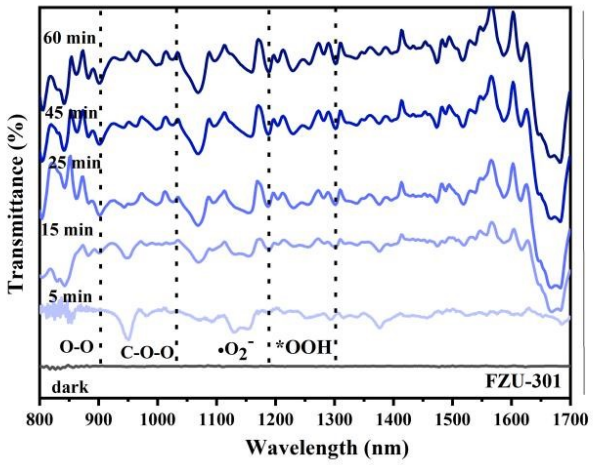


**Figure S50.** The in-situ DRIFT spectra of FZU-301.

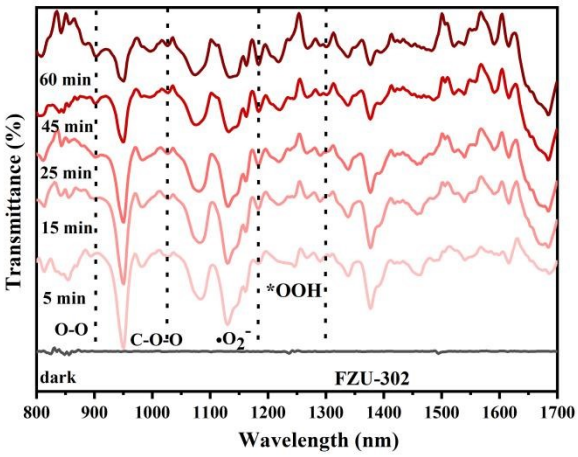


**Figure S51.** The in-situ DRIFT spectra of FZU-302.

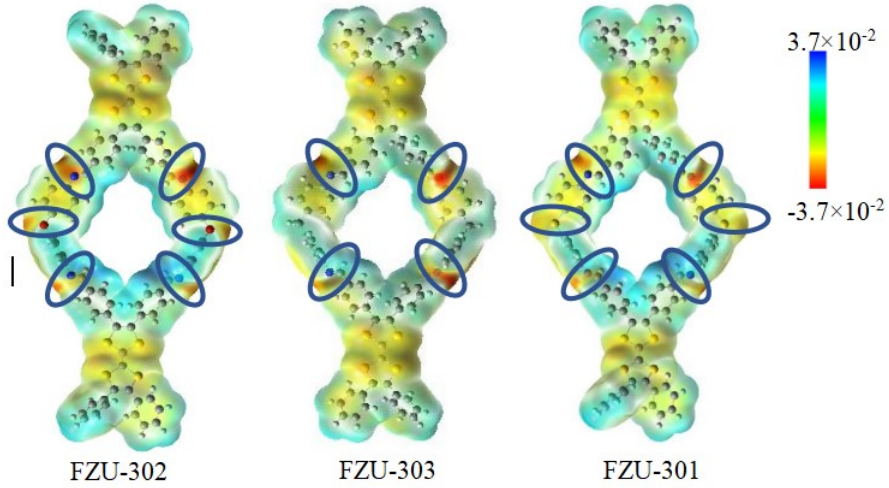


**Figure S52.** The ESP surface maps for optimized structures of FZU-301、FZU-302 and FZU-303.

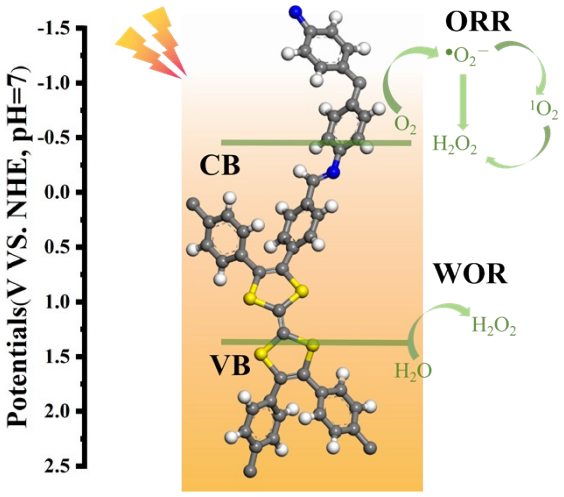


**Figure S53.** FZU-303 photocatalysis mechanism diagram.

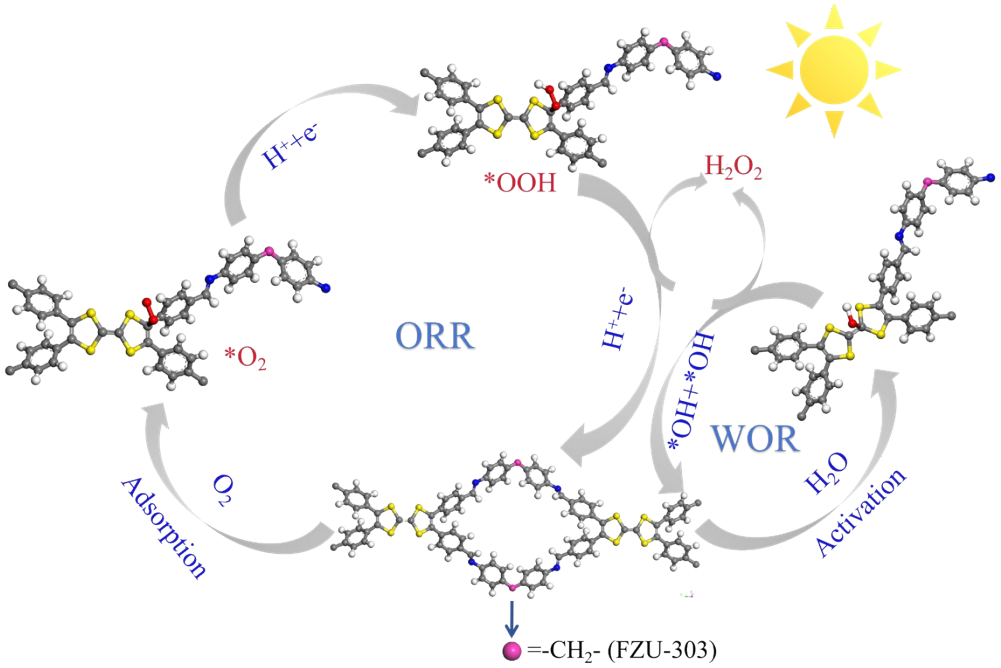


**Figure S54.** Proposed mechanism of $H_2O_2$ photosynthesis process on FZU-303.

**Table S1.** Fitted parameters and average lifetimes of fs-TAS.

| Photocatalyst | $\tau_1$ (ps) | $\tau_2$ (ps) | $\tau_{ave}$ (ps) |
|---|---|---|---|
| FZU-302 | 1.40 | 47.21 | 45.56 |
| | $R_1$: 2.88% | $R_2$: 97.12% | |
| FZU-303 | 1.33 | 86.35 | 84.80 |
| | $R_1$: 1.52% | $R_2$: 98.48% | |
| FZU-301 | 1.78 | 35.76 | 36.63 |
| | $R_1$: 4.74 % | $R_2$: 95.26% | |

$\tau_{ave} = (R_1 \times \tau_1^2 + R_2 \times \tau_2^2)/(R_1 \times \tau_1 + R_2 \times \tau_2)$.

**Table S2.** Comparison of photocatalytic $H_2O_2$ production performance of FZU-303 with reported COF photocatalysts.

| Photocatalyst | SCC | AQY (at 420 nm) | Light source | $H_2O_2$ yield ($umolg^{-1}h^{-1}$) | Solvent(s) | Ref. |
|---|---|---|---|---|---|---|
| DMAP-BNCOFs | 0.58% | 8.3% | λ>420 nm | 8051.4 | $H_2O$ | *J. Am. Chem. Soc.* 2025, 147, 24050-24059 |
| iTPPy-COF | 0.65% | 8.3% | λ>420 nm | 7955 | $H_2O$ | *Angew. Chem. Int. Ed. 2025, 64, e202425617* |
| BDT-BTT-COF | \ | 2.0% | λ>420 nm | 25670 | BnAm/Acetonitrile | *Adv. Funct. Mater. 2026; 0:e32122* |
| BDT-BT-COF | \ | \ | | 16920 | | |
| STT COF | \ | 40% | λ >320 nm | 14356.5 | $H_2O$ | *Nat. Commun., 2025, 161, 8941* |
| Hz-TP-BT-COF | \ | 15.35% | λ >300 nm | 12500 | $H_2O$ | *Nat. Catal., 2024, 72, 195-206* |
| TpAP[5] | 0.09% | 1.11% | λ>420 nm | 2343 | $H_2O$/EtOH (9/1) | *J. Am. Chem. Soc.* 2025, 147, 13618 |
| $TF_{50}$-COF | 0.17% | 5.2% at 400 nm | λ>400 nm | 1739 | $H_2O$: EtOH (9/1) | *Angew. Chem. Int. Ed.* 2022, 61, e202202328 |
| DVA-COF | 0.08% | 2.84% | 420 nm LED | 8450 | $H_2O$/benzyl alcohol (9/1) | *Angew. Chem. Int. Ed.* 2024, 63, e202402297 |
| Py-Da-COF | 0.09% | 5.4% | λ>420 nm | 1242 | $H_2O$/benzyl alcohol (9/1) | *Angew. Chem. Int. Ed.* 2023, 62, e202216719 |
| DMCR-1NH | \ | 10.0% | λ=420 -700nm | 2118 | $H_2O$/benzyl alcohol (10/1) | *J. Am. Chem. Soc.* 2023, 145, 2975 |
| sono-COF-F2 | \ | 4.8% | λ>420 nm | 414.6 | $H_2O$/benzyl alcohol (1/9) | *J. Am. Chem. Soc.* 2022, 144, 9902 |
| TAPT-FTPB COFs | 1.22% | \ | AM 1.5G | 3780 | $H_2O$ | *Nat. Synth.*, 2025, 4, 134 |
| B[f]QCOF-1 | 0.23% | 5.2% at 450 nm | λ>420 nm | 9025 | $H_2O$ | *Nat. Commun.* 2025, 16, 3493 |
| THB-COF | 0.16% | 2.11% | λ > 420 nm | 1366 | $H_2O$ | Adv. Funct. Mater. 2025, e12475 |
| THT-COF | 0.45% | 6.50% | | 5455 | | |
| HHT-COF | 0.62% | 8.77% | | 6432 | | |
| *β*-TT-TDAN COF | 1.35% | 19.20% | λ>420 nm | 3424 | $H_2O$ | *Adv. Mater.* 2025, 37, 2500913 |
| TAA-CTP-COF | \ | \ | Full spectrum | 502 | $H_2O$ | *ACS Catal.* 2024, 14, 3778 |
| FS-OHOMe-COF | 0.58% | 9.6% | λ>420 nm | 2200 | $H_2O$ | *Angew. Chem. Int. Ed.* 2024, 63, e202403926 |
| HEP-TAPT-COF | 0.65% | 15.35% | λ>420 nm | 1750 | $H_2O$ | *Angew. Chem. Int. Ed.* 2023, 62, e202217479 |
| TTF-BT-COF | 0.49% | 11.19% | λ>420 nm | 2760 | $H_2O$ | Angew. Chem. Int. Ed. 2023, 62, e202218868 |

| | | | | | | |
|---|---|---|---|---|---|---|
| Bpt-CTF | 0.2% | 8.7% | λ=350 -780nm | 3268.1 | $H_2O$ | *Adv. Mater.* 2022, 34, 2110266 |
| TD-COF | 0.15% | \ | white LED | 3364 | $H_2O$ | *Angew. Chem. Int. Ed.* 2023, 62, e202309624 |
| TT-COF | \ | \ | (400-700 nm) | 2890 | | |
| $SO_3H$-COF | 0.40% | 8.6% | λ>400 nm | 3015 | $H_2O$ | *Angew. Chem. Int. Ed.* 2024, 63, e202404077 |
| COF-BD2 | 0.68% | 18.4% at 400 nm | λ>420 nm | 5211 | $H_2O$ | *Angew. Chem. Int. Ed.* 2025, e202505621 |
| TFBP-DHBD COF | \ | \ | λ>420 nm | 1444 | $H_2O$ | *Adv. Mater.* 2025, 2502990 |
| $PD^{2+}$-$COF_{16.7}$ | 0.34% | 12.9% | λ>400 nm | 1732 | $H_2O$ | Angew. Chem. Int. Ed. 2023. 62, e202315456 |
| $COF\text{-}N_{32}$ | 0.31% | 6.2% at 459 nm | λ>420 nm | 605 | $H_2O$ | Nat Commun 14, 4344 (2023) |
| TZ-COF | 0.04% | \ | λ>420 nm | 268 | $H_2O$ | Angew. Chem. Int. Ed. 2023, 62, e202309480 |
| CTF-BDDBN | 0.14% | \ | λ>420 nm | 887 | $H_2O$ | Adv. Mater. 2020, 32, e1904433. |
| Pz-COF | 0.65% | 7.83% | λ>420 nm | 7631 | $H_2O$ | Angew. Chem. Int. Ed. 2025, e20491 |
| COF-TfpBpy | 0.57% | 8.1% | λ>420 nm | 2084 | $H_2O$ | Angew. Chem. Int. Ed. 2022, 61, e202200413 |
| PyIm-COF | 0.25% | 3.7% | λ>420 nm | 5850 | $H_2O$ | Angew. Chem. Int. Ed. 2024, 63, e202404563 |
| TACOF-1-COOH | 0.55% | 5.7% | λ>420 nm | 3542 | $H_2O$ | Angew. Chem. Int. Ed. 2024, 63, e202408802 |
| DQTb-COFs | 0.21% | 2.1% | λ>400 nm | 1844 | $H_2O$ | Chem. Eng. J. 2024, 481, 148494 |
| Py-Da-COF | 0.09% | 4.5% | λ>420 nm | 461 | $H_2O$ | Angew. Chem. Int. Ed. 2023, 62, e202216719 |
| ECUT-COF-50 | 0.52% | 9.1% at 400 nm | λ>400 nm | 2448 | $H_2O$ | Angew. Chem. Int. Ed. 2024, e202414658 |
| ECUT-COF-50 | 0.68% | 11.2% at 400 nm | | 4742 | | |
| Bpy-TAPT | 0.65% | 8.6% | λ>420 nm | 4038 | $H_2O$ | Appl. Catal. B-Environ. 2020, 272, 118970 |
| COF-2CN | 0.6% | 6.8% | λ>420 nm | 1601 | $H_2O$ | Angew. Chem. Int. Ed. 2024, 63, e202318562 |
| FS-COFs | \ | 6.21% | λ>420 nm | 3904.2 | $H_2O$ | Angew. Chem. Int. Ed. 2023, 62, e202305355 |
| FZU-303 | 0.95% | 7.4% | λ>420 nm | 4642 | $H_2O$ | This work |

**Table S3.** Comparison of exciton binding energy and $H_2O_2$ production of 1D COFs with other reported COFs photocatalysts.

| COF | Exciton binding energy (emV) | $H_2O_2$ Photocatalytic performance ($umolg^{-1}h^{-1}$) | Ref |
|---|---|---|---|
| COF-2CN | 67.6 | 1601 | Angew. Chem. Int. Ed. 2024, 63, e202318562 |
| COF-1CN | 79.3 | 573 | |
| COF-0CN | 86.2 | 194 | |
| BTBpy | 44.2 | 441 | Nat Commun 16, 7432 (2025) |
| COF-OUT-1 | 53.9 | 983 | Angew. Chem. Int. Ed. 2025, 64, e202510293 |
| COF-OUT-2 | 49.6 | 2351 | |
| COF-1N-1 | 36.4 | 5463 | |
| ECUT-COF-50 | 32.4 | 4742 | Angew. Chem. Int. Ed. 2024, e202414658 |
| ECUT-COF-51 | 89.1 | 2448 | |
| FS-OHOMe-COF | 65.8 | 1480 | Angew. Chem. Int. Ed. 2024, 63, e202403926 |
| FS-OH-COF | 113.3 | 780 | |
| FS-OMe-COF | 72.9 | 1150 | |
| TMB-COF-4 | 44.7 | 5106 | Angew. Chem. Int. Ed. 2024, 64, e202412890 |
| TMB-COF-3 | 52.4 | 2621 | |
| TMB-COF-2 | 65.6 | 1293 | |
| TMB-COF-1 | 67.1 | 218 | |
| BBT CAN COF-1 | 36.2 | 2500 | Adv. Funct. Mater. 2025, 2424035 |
| BBT CAN COF-2 | 149 | 910 | |
| FZU-303 | 33.4 | 4642 | This Work |
| FZU-302 | 44.6 | 1547 | |
| FZU-301 | 48.8 | 1032 | |

**Table S4.** Fractional atomic coordinates for the unit cell of FZU-301 with AA stacking.

| Space group: P2 | | | |
|---|---|---|---|
| a = 24.834 b = 4.767 c = 26.371 α = β = γ = 90° | | | |
| Atom | x | y | z |
| C1 | -5.579 | -1.815 | -19.784 |
| C2 | -6.931 | -1.819 | -19.801 |
| S3 | -4.642 | -1.79 | -18.24 |
| C4 | -3.106 | -1.336 | -19.07 |
| C5 | -3.088 | -1.323 | -20.423 |
| S6 | -4.612 | -1.717 | -21.304 |
| S7 | -7.864 | -1.749 | -21.346 |
| C8 | -9.397 | -1.301 | -20.508 |
| C9 | -9.42 | -1.331 | -19.155 |
| S10 | -7.904 | -1.779 | -18.282 |

| | | | |
|---|---|---|---|
| C11 | -10.61 | -1.023 | -18.315 |
| C12 | -10.523 | -0.834 | -21.362 |
| C13 | -1.967 | -0.91 | -18.212 |
| C14 | -1.897 | -1.007 | -21.257 |
| C15 | -11.88 | -1.536 | -18.626 |
| C16 | -12.982 | -1.252 | -17.824 |
| C17 | -12.844 | -0.449 | -16.686 |
| C18 | -11.581 | 0.068 | -16.362 |
| C19 | -10.471 | -0.22 | -17.168 |
| C20 | -10.827 | -1.48 | -22.574 |
| C21 | -11.914 | -1.056 | -23.355 |
| C22 | -12.688 | 0.044 | -22.951 |
| C23 | -12.364 | 0.702 | -21.759 |
| C24 | -11.269 | 0.292 | -20.998 |
| C25 | -1.209 | 0.215 | -18.55 |
| C26 | -0.098 | 0.586 | -17.794 |
| C27 | 0.23 | -0.112 | -16.625 |
| C28 | -0.558 | -1.211 | -16.245 |
| C29 | -1.659 | -1.597 | -17.025 |
| C30 | -2.025 | -0.151 | -22.367 |
| C31 | -0.913 | 0.146 | -23.167 |
| C32 | 0.339 | -0.415 | -22.875 |
| C33 | 0.465 | -1.271 | -21.774 |
| C34 | -0.638 | -1.563 | -20.977 |
| C35 | -14.035 | -0.189 | -15.86 |
| C36 | -13.809 | 0.56 | -23.763 |
| C37 | 1.363 | 0.366 | -15.808 |
| C38 | 1.534 | -0.14 | -23.691 |
| S39 | -18.715 | 1.602 | -28.562 |
| C40 | -20.092 | 1.267 | -27.428 |
| C41 | -17.353 | 1.154 | -27.454 |
| C42 | -21.266 | 2.024 | -27.519 |
| C43 | -22.332 | 1.786 | -26.637 |
| C44 | -22.245 | 0.771 | -25.675 |
| C45 | -21.086 | -0.027 | -25.634 |
| C46 | -20.028 | 0.217 | -26.506 |
| C47 | -17.238 | 1.749 | -26.193 |
| C48 | -16.205 | 1.38 | -25.327 |
| C49 | -15.267 | 0.4 | -25.713 |
| C50 | -15.4 | -0.201 | -26.971 |
| C51 | -16.423 | 0.188 | -27.847 |
| N52 | -23.362 | 0.538 | -24.8 |
| N53 | -14.192 | -0.032 | -24.857 |

| | | | |
|---|---|---|---|
| S54 | -18.623 | 1.295 | -10.925 |
| C55 | -19.964 | 0.864 | -12.068 |
| C56 | -17.236 | 1.018 | -12.062 |
| C57 | -20.886 | -0.124 | -11.719 |
| C58 | -21.897 | -0.495 | -12.618 |
| C59 | -22.021 | 0.144 | -13.857 |
| C60 | -21.084 | 1.138 | -14.205 |
| C61 | -20.066 | 1.49 | -13.315 |
| C62 | -17.272 | -0.019 | -12.999 |
| C63 | -16.212 | -0.216 | -13.88 |
| C64 | -15.08 | 0.619 | -13.832 |
| C65 | -15.017 | 1.619 | -12.853 |
| C66 | -16.087 | 1.811 | -11.964 |
| N67 | -23.095 | -0.258 | -14.73 |
| N68 | -13.963 | 0.429 | -14.718 |

**Table S5.** Fractional atomic coordinates for the unit cell of FZU-302 with AA stacking.

| Space group: P2 | | | |
|---|---|---|---|
| a = 25.811 b = 4.310 c = 28.768 α = β = γ = 90° | | | |
| C1 | 6.201 | 4.202 | 22.036 |
| C2 | 7.539 | 4.3 | 22.104 |
| S3 | 5.301 | 4.34 | 20.478 |
| C4 | 3.689 | 4.148 | 21.243 |
| C5 | 3.625 | 4.057 | 22.596 |
| S6 | 5.183 | 3.9 | 23.493 |
| S7 | 8.457 | 4.273 | 23.647 |
| C8 | 10.073 | 4.343 | 22.818 |
| C9 | 10.095 | 4.351 | 21.454 |
| S10 | 8.525 | 4.495 | 20.611 |
| C11 | 11.289 | 4.148 | 20.556 |
| C12 | 11.257 | 4.52 | 23.707 |
| C13 | 2.54 | 4.326 | 20.316 |
| C14 | 2.376 | 4.028 | 23.438 |
| C15 | 1.484 | 5.14 | 20.684 |
| C16 | 0.411 | 5.39 | 19.852 |
| C17 | 0.386 | 4.863 | 18.56 |
| C18 | 1.463 | 4.053 | 18.14 |
| C19 | 2.529 | 3.77 | 19.026 |
| C20 | 1.215 | 3.365 | 23.033 |
| C21 | 0.145 | 3.166 | 23.895 |

| | | | |
|---|---|---|---|
| C22 | 0.116 | 3.782 | 25.144 |
| C23 | 1.203 | 4.592 | 25.514 |
| C24 | 2.339 | 4.683 | 24.679 |
| C25 | 11.297 | 4.609 | 19.224 |
| C26 | 12.387 | 4.36 | 18.377 |
| C27 | 13.494 | 3.645 | 18.848 |
| C28 | 13.488 | 3.17 | 20.161 |
| C29 | 12.397 | 3.419 | 20.982 |
| C30 | 11.255 | 4.025 | 25.024 |
| C31 | 12.34 | 4.277 | 25.874 |
| C32 | 13.411 | 5.053 | 25.419 |
| C33 | 13.424 | 5.529 | 24.118 |
| C34 | 12.374 | 5.243 | 23.278 |
| C35 | -0.808 | 5.162 | 17.735 |
| C36 | 14.665 | 3.4 | 18.001 |
| C37 | 14.594 | 5.276 | 26.22 |
| C38 | -1.069 | 3.556 | 26.002 |
| O39 | 19.64 | 4.286 | 30.08 |
| C40 | 20.872 | 4.174 | 29.382 |
| C41 | 18.472 | 4.319 | 29.313 |
| C42 | 21.932 | 5.02 | 29.732 |
| C43 | 23.095 | 5.092 | 28.938 |
| C44 | 23.243 | 4.261 | 27.811 |
| C45 | 22.166 | 3.426 | 27.457 |
| C46 | 21.02 | 3.362 | 28.254 |
| C47 | 18.42 | 4.918 | 28.058 |
| C48 | 17.208 | 5.086 | 27.432 |
| C49 | 16.03 | 4.571 | 28.008 |
| C50 | 16.102 | 3.894 | 29.231 |
| C51 | 17.316 | 3.848 | 29.911 |
| N52 | 24.425 | 4.359 | 26.983 |
| N53 | 14.795 | 4.594 | 27.302 |
| O54 | 19.663 | 4.345 | 13.997 |
| C55 | 20.9 | 4.483 | 14.692 |
| C56 | 18.464 | 4.151 | 14.712 |
| C57 | 22.051 | 3.984 | 14.065 |
| C58 | 23.31 | 4.014 | 14.685 |
| C59 | 23.448 | 4.62 | 15.941 |
| C60 | 22.304 | 5.202 | 16.54 |
| C61 | 21.053 | 5.152 | 15.916 |
| C62 | 18.445 | 3.61 | 15.999 |
| C63 | 17.268 | 3.561 | 16.72 |
| C64 | 16.065 | 4.014 | 16.141 |

| | | | |
|---|---|---|---|
| C65 | 16.062 | 4.459 | 14.81 |
| C66 | 17.264 | 4.496 | 14.095 |
| N67 | 24.718 | 4.543 | 16.622 |
| N68 | 14.854 | 4.071 | 16.904 |

**TableS6.** Fractional atomic coordinates for the unit cell of FZU-303 with AA stacking.

| Space group: P2 | | | |
|---|---|---|---|
| a = 25.753 b = 4.625 c = 24.876 α = β = γ = 90° | | | |
| C1 | 5.749 | 6.556 | 18.662 |
| C2 | 7.12 | 6.557 | 18.651 |
| S3 | 4.776 | 6.569 | 17.122 |
| C4 | 3.31 | 5.898 | 17.946 |
| C5 | 3.346 | 5.787 | 19.305 |
| S6 | 4.861 | 6.248 | 20.198 |
| S7 | 8.092 | 6.57 | 20.192 |
| C8 | 9.559 | 5.9 | 19.367 |
| C9 | 9.523 | 5.788 | 18.009 |
| S10 | 8.007 | 6.249 | 17.116 |
| C11 | 10.669 | 5.297 | 17.198 |
| C12 | 10.744 | 5.561 | 20.229 |
| C13 | 2.125 | 5.559 | 17.084 |
| C14 | 2.2 | 5.296 | 20.116 |
| C15 | 0.885 | 6.168 | 17.288 |
| C16 | -0.181 | 5.966 | 16.419 |
| C17 | -0.091 | 5.043 | 15.379 |
| C18 | 1.105 | 4.337 | 15.222 |
| C19 | 2.223 | 4.64 | 16.025 |
| C20 | 1.497 | 4.173 | 19.714 |
| C21 | 0.297 | 3.809 | 20.335 |
| C22 | -0.168 | 4.5 | 21.453 |
| C23 | 0.607 | 5.564 | 21.94 |
| C24 | 1.792 | 5.943 | 21.287 |
| C25 | 11.076 | 5.944 | 16.027 |
| C26 | 12.261 | 5.564 | 15.374 |
| C27 | 13.035 | 4.5 | 15.86 |
| C28 | 12.57 | 3.809 | 16.978 |

| | | | |
|---|---|---|---|
| C29 | 11.372 | 4.174 | 17.6 |
| C30 | 10.646 | 4.641 | 21.288 |
| C31 | 11.764 | 4.338 | 22.091 |
| C32 | 12.959 | 5.045 | 21.936 |
| C33 | 13.049 | 5.969 | 20.896 |
| C34 | 11.984 | 6.17 | 20.026 |
| C35 | -1.239 | 4.898 | 14.464 |
| C36 | 14.285 | 4.043 | 15.201 |
| C37 | 14.107 | 4.9 | 22.852 |
| C38 | -1.418 | 4.043 | 22.111 |
| C39 | 19.362 | 3.17 | 26.506 |
| C40 | 20.604 | 3.488 | 25.694 |
| C41 | 18.06 | 3.361 | 25.722 |
| C42 | 21.543 | 4.433 | 26.128 |
| C43 | 22.609 | 4.802 | 25.288 |
| C44 | 22.801 | 4.182 | 24.038 |
| C45 | 21.903 | 3.169 | 23.653 |
| C46 | 20.831 | 2.828 | 24.483 |
| C47 | 17.959 | 4.3 | 24.686 |
| C48 | 16.803 | 4.402 | 23.909 |
| C49 | 15.67 | 3.608 | 24.175 |
| C50 | 15.774 | 2.645 | 25.2 |
| C51 | 16.94 | 2.555 | 25.991 |
| N52 | 23.928 | 4.578 | 23.227 |
| N53 | 14.442 | 3.768 | 23.408 |
| C54 | 19.258 | 3.169 | 10.809 |
| C55 | 20.56 | 3.36 | 11.592 |
| C56 | 18.016 | 3.488 | 11.62 |
| C57 | 21.681 | 2.554 | 11.323 |
| C58 | 22.847 | 2.644 | 12.114 |
| C59 | 22.951 | 3.606 | 13.139 |
| C60 | 21.818 | 4.4 | 13.405 |
| C61 | 20.662 | 4.299 | 12.628 |
| C62 | 17.79 | 2.829 | 12.832 |
| C63 | 16.718 | 3.169 | 13.661 |
| C64 | 15.82 | 4.183 | 13.275 |
| C65 | 16.012 | 4.803 | 12.026 |
| C66 | 17.077 | 4.433 | 11.186 |
| N67 | 24.179 | 3.766 | 13.905 |
| N68 | 14.694 | 4.579 | 14.087 |

## References

[1] K. Lin, J. Wang, S. Qiao, Z. Guo, *ACS Sustainable Chemistry & Engineering.* **2024**, 12, 6719-6727.

[2] J. N. Chang, Q. Li, J. W. Shi, M. Zhang, L. Zhang, S. Li, Y. Chen, S. L. Li, Y. Q. Lan, *Angewandte Chemie International Edition.* **2023**, 62, 202218868.

[3] J. Y. Yue, J. X. Luo, Z. X. Pan, R. Z. Zhang, P. Yang, Q. Xu, B. Tang, *Angewandte Chemie International Edition.* **2024**, 63, 5202405763.

[4] J.-Y. Yue, L.-P. Song, Z.-X. Pan, M. Cheng, X. Wang, Q. Xu, P. Yang, *Chemical Engineering Journal.* **2025**, 504, 158983.

[5] X. Ma, S. Li, Y. Gao, N. Li, Y. Han, H. Pan, Y. Bian, J. Jiang, *Advanced Functional Materials.* **2024**, 34, 2409913.

[6] G. Kresse, J. Hafner, Ab initio molecular dynamics for liquid metals. *Physical Review B*. **1993**, 47, 558-561.

[7] G. Kresse, J. Furthmüller, Efficiency of ab-initio total energy calculations for metals and semiconductors using a plane-wave basis set. *Computational Materials Science.* **1996**, 6, 15-50.

[8] J. P. Perdew, K. Burke, M. Ernzerhof, Generalized Gradient Approximation Made Simple, *Physical Review Letters*. **1996**, 77, 3865-3868.

[9] P. E. Blöchl, Projector augmented-wave method. *Physical Review B*. **1994**, 50, 17953-17979.

[10] S. Grimme, Semiempirical GGA-type density functional constructed with a long-range dispersion correction, *Journal of Computational Chemistry*. **2006**, 27, 1787–1799.

[11] G. Henkelman, A. Arnaldsson, and H. Jónsson, A fast and robust algorithm for Bader decomposition of charge density, *Computational Materials Science*. **2006**, 36, 354-360.